Temperature-induced prophage dictates evolution of virulence in bacteria

Matthieu Bruneaux[1*], Roghaieh Ashrafi[1], Ilkka Kronholm[1], Elina Laanto[1,2], Anni-Maria Örmälä-Odegrip[3], Juan A. Galarza[1], Chen Zihan[1,4], Mruthyunjay Kubendran Sumathi[1,5], Tarmo Ketola[1]

October 29, 2021

[1]Department of Biological and Environmental Science, University of Jyväskylä, Finland.
[2]Molecular and Integrative Biosciences Research Programme, Faculty of Biological and Environmental Sciences, University of Helsinki, Finland.
[3]Department of Laboratory Medicine, Karolinska Institute, Stockholm, Sweden.
[4]Current address: Shenzhen Research Institute, The Chinese University of Hong Kong, China.
[5]Current address: Department of Ecology and Evolutionary Biology, University of Arizona, Tucson, USA.
[*]Corresponding author: Matthieu Bruneaux, matthieu.bruneaux@ens-lyon.org

Abstract

Environmental changes can cause strong cascading effects in species communities through altered species interactions. The highly specialized interactions arising from the co-evolution of hosts and parasites such as bacteria and phages as well as their short generation times can rapidly lead to considerable evolutionary responses to abiotic changes, with potential large-scale ramifications to other trophic levels. Here we report how the temperature-dependent induction of a temperate phage in the bacterium *Serratia marcescens* resulted in both genetic and epigenetic changes in the bacterial host after experimental evolution under different temperatures, and subsequently altered the virulence of the bacterium itself in an insect host. The majority of the genetic and epigenetic changes were associated with the indirect effects of the phage on the bacterium rather than with the experimentally imposed thermal environments. Given the abundance of temperate phages in bacterial genomes, the sensitivity of the onset of their lytic cycle to environmental conditions, and the predominance of environmental changes due to climate change, our results warrant attention as a cautionary example of the dangers of predicting environmental effects on species without considering complex biotic interactions.

Keywords: prophage induction, epigenetics, experimental evolution, opportunistic pathogen.

Introduction

Understanding the consequences of environmental changes on ecosystems is of high priority as climate change alters environmental conditions (Chevin et al., 2010; Kristensen et al., 2020). Abiotic environmental selection pressures can affect species directly or indirectly via their ecological interactions with other more sensitive species. Understanding those indirect effects is critical as they can amplify through ecosystems (Zarnetske et al., 2012) and requires studying multi-species systems rather than focusing on single species. In this respect, phage-bacteria systems are both relevant for natural ecosystems and practical for laboratory experiments. Phages are ubiquitous pathogens that can drive the abundance and composition of bacterial communities (Suttle, 2005). Many phages exist as inducible prophages present in bacterial genomes and environmental perturbations can trigger their induction (Canchaya et al., 2003; Williamson et al., 2002; Brum et al., 2016; Howard-Varona et al., 2017). Since bacteria have a key role in nutrient and energy cycles, indirect consequences of prophage induction can range from modulation of biogeochemical cycles (Suttle, 2005) to life and death of multicellular hosts of pathogenic bacteria (Buck and Ripple, 2017).

We used an evolution experiment and single-molecule real-time (SMRT) sequencing to determine the effects of temperature changes on the evolution of a bacterium (*Serratia marcescens*) carrying a temperature-sensitive prophage. We describe a novel trophic cascade where prophage induction directed the evolution of its bacterial host, and show that prophage-driven evolution cascaded across trophic levels by having strong effects on bacterial virulence in an insect host. While a previous study showed that temperature, the main selective pressure imposed on bacterial populations in the evolution experiment, was not strongly associated with genetic or epigenetic changes (Bruneaux et al., 2021), we found here that many genetic and epigenetic differences observed between bacteria genomes were prophage-related.

Results and Discussion

S. marcescens carries a temperature-inducible prophage

Serratia marcescens is an environmental pathogen that is virulent in many invertebrate species and responsible for nosocomial infections in humans (Flyg et al., 1980; Grimont and Grimont, 2006). In-silico analysis predicted the existence of five prophage candidates inside the genome of the strain used in our study (ATCC 13880), two of which were predicted to lack some features essential for phage production (based on the PHASTER tool (Arndt et al., 2016); Supplementary Table S1). To test if some of the prophages were sensitive to environmental conditions, we implemented a method based on quantitative polymerase chain reaction (qPCR) to estimate the rate of induction of the candidate prophages in bacterial cultures by quantifying extracellular, DNase-resistant prophage sequences which we assumed to be contained inside released phage particles. We used this method on *S. marcescens* cultures under a range of temperature assays to determine whether the prophage candidates could be environmentally induced. The only extracellular prophage sequence detected in our assays was from prophage candidate PP4 (see reference strain results in Figure 1). PP4 showed significant sequence similarity to the *S. marcescens* phage KSP20 previously isolated from aquatic environment (Matsushita et al., 2009) and to P2-like temperate phages and prophages from Enterobacterales (Supplementary Figure S1).

We performed two additional experiments using different approaches to confirm the induction of PP4 phage particles detected with our qPCR method. The first approach was to search for phage particles from pellets prepared from the supernatant of a reference strain culture grown at 31 °C using transmission electron microscopy (TEM). Particles of shape and size compatible with a P2-like phage were successfully observed, albeit in low frequency (Figure 2). The phage identity was confirmed by qPCR using PP4-specific primers on the TEM pellets. The second approach consisted in plaque assays with supernatants from reference strain cultures spread onto lawn cultures of

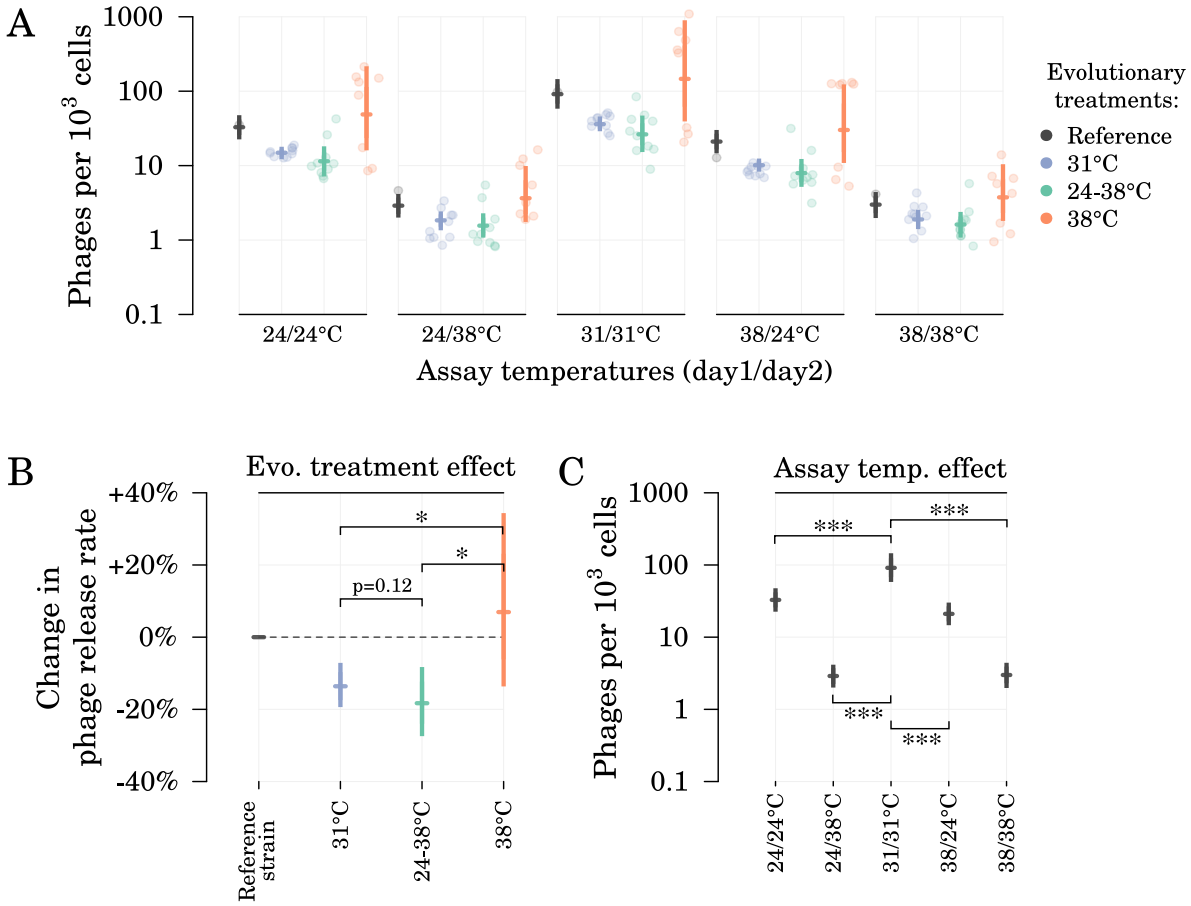

Figure 1: Effect of evolutionary treatment and assay temperatures on the estimated induction of prophage PP4. Assays lasted two days and assay temperatures are given as day1/day2. A) posteriors of the model-estimated mean for each treatment/assay combination. Points are estimated phage release rates for each of the 29 sequenced clones. B) estimates of the evolutionary treatment effects and C) estimates of the assay effects, with the reference strain used as a reference point. Posteriors are shown as median and 95% credible interval. One-sided Bayesian p-values for pairwise comparisons denoted by * ($p < 0.05$) and *** ($p < 0.001$). Full posterior estimates for individual strains are shown in Supplementary Figure S3.

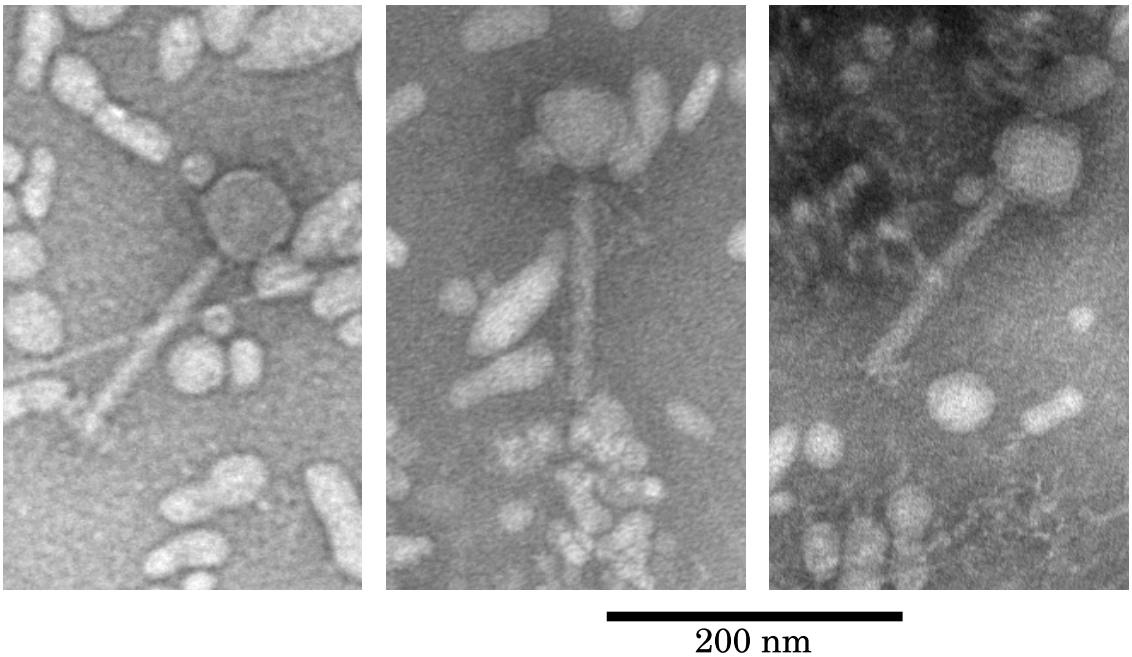

Figure 2: Putative PP4 phage particles observed in transmission electron microscopy (TEM). Negative staining with phosphotungstic acid (PTA) was used. All panels are shown to the same scale.

several candidate strains, including the reference strain, but no plaque was observed in any of the conditions tested. Taken together, those results confirm that the PP4 prophage is induced in *S. marcescens* cells and released as phage particles at a low rate, as detected by qPCR and confirmed by TEM, and that the induction and/or infectivity rates of this phage are low enough that no clearing is observed in our plaque assays. Interestingly, the immunity repressor protein located immediately upstream of the PP4 integrase is of the short type (99 amino-acid long) and thus most likely of the P2-type rather than of the longer 186-type (Christie and Calendar, 2016). Since phage 186 is inducible by the SOS response while phage P2 is not, this suggests that prophage PP4 might be non-inducible by the SOS response similarly to P2 (Christie and Calendar, 2016; Lamont et al., 1989).

Abiotic changes affect the evolution of prophage-bacteria interaction

The induction of prophage PP4 as estimated by our method was more pronounced in the reference strain at 24 °C and 31 °C rather than at 38 °C. This environmental sensitivity suggested that cooler environments could act as a strong selective force in *S. marcescens* as evolution in cooler environments could potentially trigger counter-adaptations in bacteria to reduce the fitness loss due to prophage induction and cell lysis (Canchaya et al., 2003), while evolution in warmer environments could on the contrary release selective pressure against such fitness loss.

To test if environmental changes could affect the relationship between prophage PP4 and its bacterial host, we used bacterial strains from an earlier experimental evolution study where temperature had been manipulated (Ketola et al., 2013): cultures of *S. marcescens* had been left to evolve under either (i) constant moderate temperature at 31 °C, (ii) constant high temperature at 38 °C, or (iii) daily fluctuating temperature between 24 and 38 °C (Supplementary Figure S2). We selected several independently evolved clones from each evolutionary treatment (n = 10, 8, and 10, respectively) and measured prophage PP4 induction with two-day thermal assays (Figure 1A). The thermal assays were (daily temperatures given for first/second day) 24/24 °C, 24/38 °C, 31/31 °C, 38/24 °C and 38/38 °C, thus enabling to test both the effect of mean temperature and of temperature fluctuations on prophage induction.

As hypothesized, we found an evolutionary adjustment of the prophage induction in cooler environments (evolutionary treatment effect, Figure 1B). The strains evolved at 31 °C and at 24-38 °C released 19% and 24% less phages, respectively, than strains evolved at 38 °C. Mean patterns of PP4 induction did not differ significantly between strains that had evolved at lower mean temperature (31 °C versus 24-38 °C). The main driver of prophage induction in our assays was the temperature of the final day of the assay, rather than whether a temperature change was experienced during the assay (assay temperatures effect, Figure 1C). Ending an assay at 31 °C induced about three times more phages than ending an assay at 24 °C, and ending an assay at 24 °C induced

about ten times more phages than ending an assay at 38 °C. Higher prophage induction rates at lower assay temperature are likely to have an adverse effect on bacterial fitness in laboratory culture conditions via cell lysis. The evolution of lower prophage induction rates in the evolutionary treatments where those temperatures occurred is consistent with such a temperature-dependent effect of PP4 on *S. marcescens* fitness.

Induced evolutionary changes have indirect consequences for bacteria's hosts

After confirming the evolutionary changes in the interaction between prophage PP4 and its bacterial host, we explored how these environmentally-triggered changes might cascade to another trophic level: a host of the bacterium itself. We estimated the virulence of the experimentally evolved strains in an insect host by measuring the survival time of waxmoth larvae (*Galleria mellonella*) infected by an injection of 5 µl of bacterial cultures and placed into two assay environments: 24 °C and 31 °C (Supplementary Figure S4). We did not use 38 °C as this temperature would have been lethal to waxmoth larvae. Control larvae were injected with sterile water and sterile medium. We estimated the relative virulences of sequenced strains from larvae survival data with a Cox proportional hazards mixed model which controlled for larva body mass and for the initial density of the bacterial cultures and which allowed for different variances across evolutionary treatments (Figure 3A). Those estimates revealed that the average virulence of clones evolved at high temperature (38 °C) tended to be higher than for clones evolved at lower mean temperature when larvae were incubated at 24 °C (38 °C versus 24-38 °C, one-sided Bayesian p-value $= 0.057$; 38 °C versus 31 °C, $p = 0.066$; Figure 3B). However, when larvae were incubated at 31 °C, these differences disappeared while clones evolved at 31 °C were more virulent than those evolved at 24-38 °C ($p < 0.01$). To confirm those tentative results obtained from the 29 sequenced clones, we utilized a much larger pool of evolved clones which confirmed that overall clones evolved at 38 °C had indeed a higher virulence than the others when assayed at room temperature ($p < 0.01$ for comparisons of 38 °C clones with both 24-38 °C and 31 °C

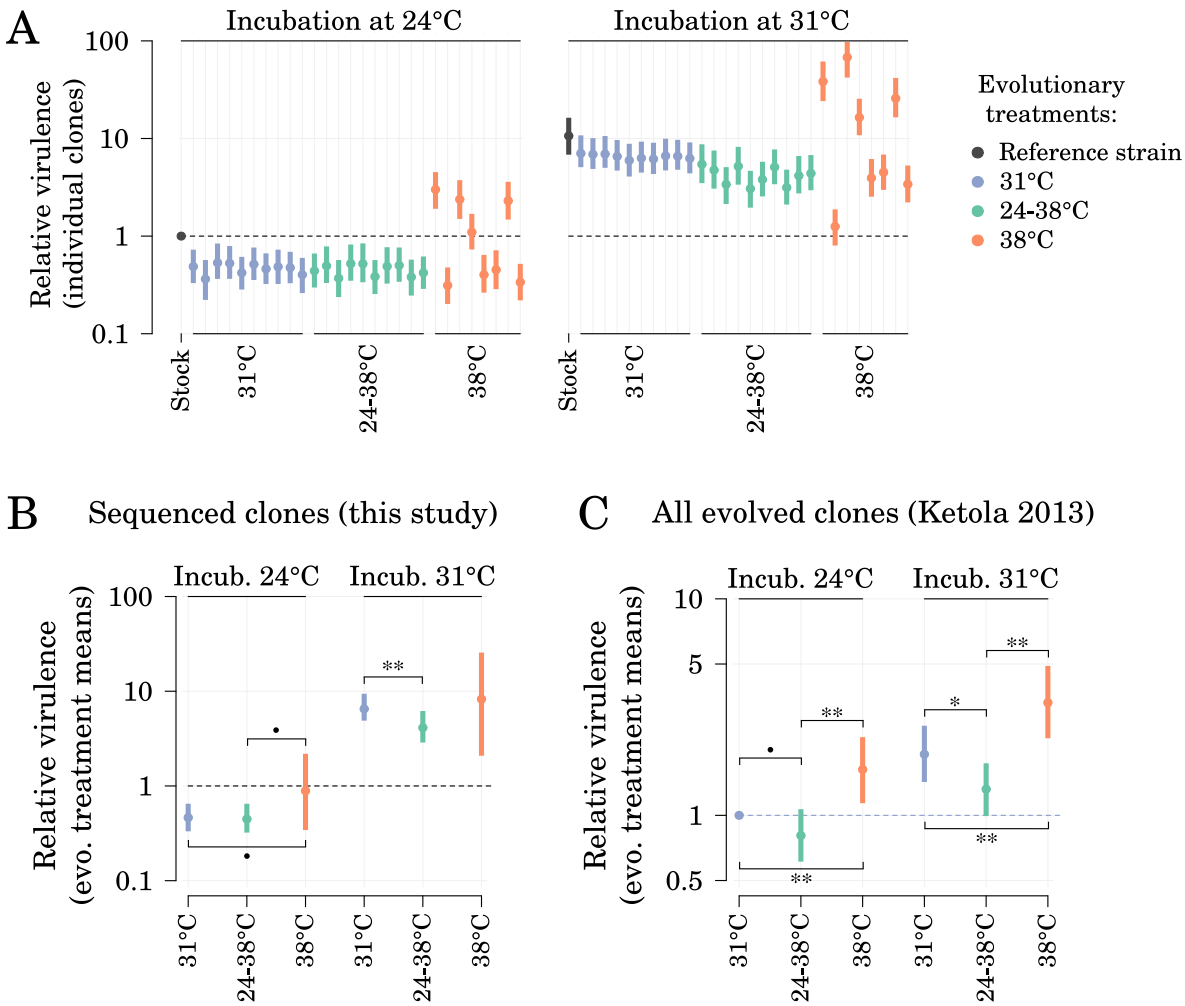

Figure 3: Effect of evolutionary treatment on strains virulence in waxmoth larvae at two incubation temperatures. A) relative virulence of individual clones, measured as relative hazards estimated from a Bayesian implementation of a Cox proportional-hazards model. All virulence estimates are relative to the virulence of the reference strain in incubation at 24 °C (denoted by a broken horizontal line) and are corrected for the effects of injection batch, larval body mass and optical density of injected cultures. B) Mean relative virulence per evolutionary treatment and per incubation temperature as estimated by the model ($\exp(\mu_{evo})$) ($n = 29$ sequenced clones). C) Confirmatory results from a similar virulence experiment utilizing more bacterial clones from the same original evolution experiment ($n = 222$ clones, virulence relative to the average virulence of the clones evolved at 31 °C when incubated at 24 °C). For each model parameter, 95 % credible interval and median of the posterior are shown.

clones, Figure 3C). This experiment also confirmed that the clones randomly chosen for sequencing were broadly representative of the larger pool of clones isolated from the evolved populations. Decreased virulence of the bacteria in the insect host accompanied with decreased prophage induction when cultivated outside of the host suggests that prophage induction closely relates to the bacteria virulence in the insect host. This was supported by the correlation between average strain virulence in waxmoth larvae and average PP4 induction rates (Spearman's $\rho = 0.52$, $p = 0.004$).

Both genetic and epigenetic variation can have a role in phenotypic changes

To explore the mechanistic basis of the evolutionary changes in prophage induction rate and in bacteria virulence and the connection between those two traits, we analysed the genomic data of the 28 evolved strains used in our study and of the reference strain pre-existing the evolution experiment. Sequencing was performed with the PacBio SMRT platform and is described in detail in a companion study (Bruneaux et al., 2021).

We did not find any known virulence factors among the identified proteins of PP4, but it should be noted that 12 of its 44 predicted proteins were unannotated (Figure S1). Some accessory proteins found in P2-related phages are known to contribute to bacterial virulence, protection against other bacteriophages or SOS prophage induction (Christie and Calendar, 2016). More generally, prophage-encoded virulence factors are considered one of the benefits brought by prophages to their bacterial host explaining the maintenance of prophages in bacterial genomes (Fortier and Sekulovic, 2013; Koskella and Brockhurst, 2014). Another possible connection between prophage induction and bacterial virulence is via the release of endotoxins upon cell lysis that could be a causative agent of *S. marcescens* virulence since its lysates are known to be cytotoxic on their own (Petersen and Tisa, 2012). Structural proteins were well conserved between PP4 and related sequences, as is common for P2-like phages (Nilsson and Haggård-Ljungquist, 2007), with the exception of tail fiber proteins (Figure S1). Tail fiber proteins are known to be involved in phage host specificity (Scholl et al.,

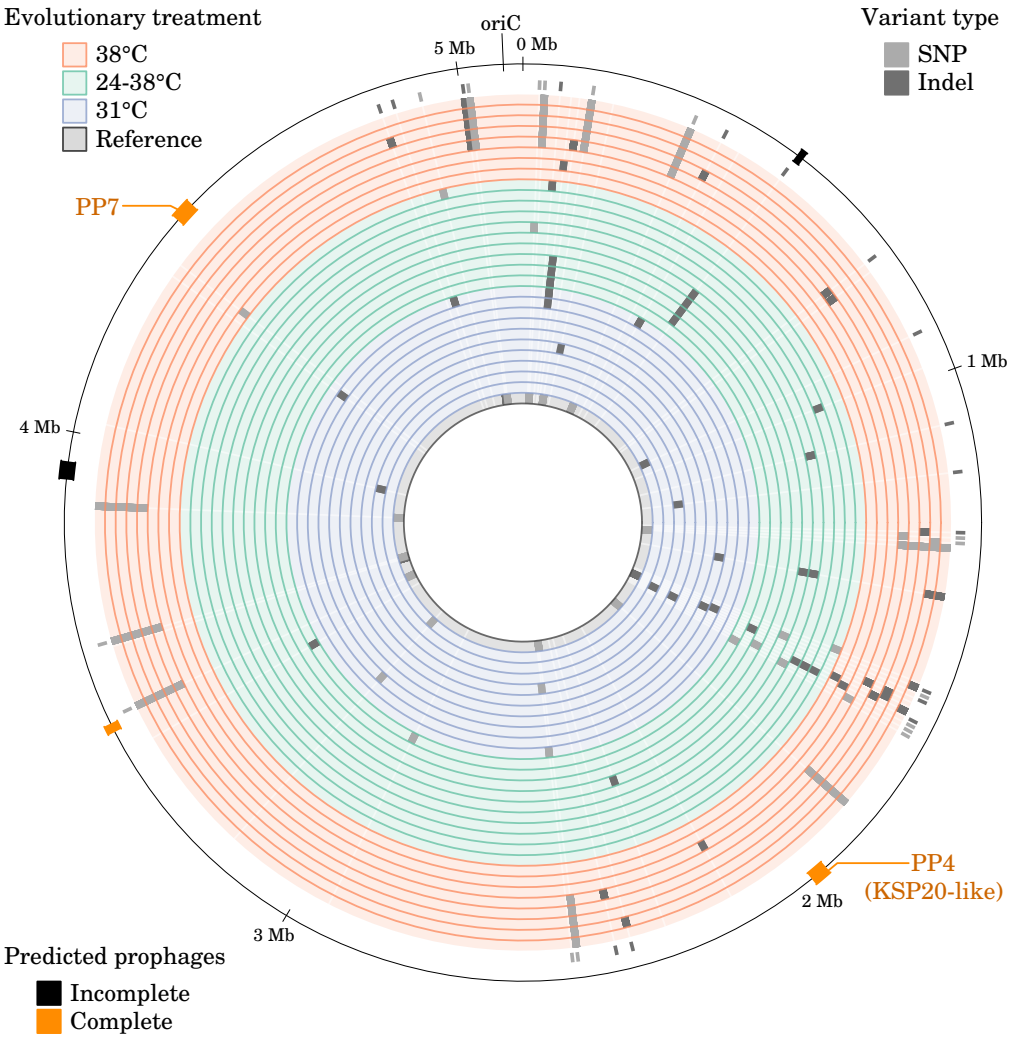

Figure 4: Alignment of the genomes from the 29 sequenced strains showing the variable genetic loci. Each circular track represents a sequenced genome, for which the evolutionary treatment is color-coded. Minor alleles for genetic variants are shown on the genome tracks in light grey (SNP) and dark grey (indels). Ticks outside the last genome track indicate non-synonymous variants (i.e. non-synonymous SNPs and indels resulting in a frame shift). The outer line represents coordinates along the genome and the locations of the five predicted prophages. Prophages PP4 and PP7 are the prophages shown in Figure S1.

Figure 5: Association between phenotypes and genetic variants observed in at least two sequenced strains. A) Distribution of genetic variants across evolutionary treatments and association between alleles and phenotypes based on Wilcoxon rank sum tests. Variant IDs can be matched with those in Supplementary Table S2 for details. B) Visualization of the association between phenotypic values and major (M) and minor (m) alleles of variant *a* and of the "pooled" variants for galactokinase and glycosyl-transferase. Colors correspond to the evolutionary treatment applied to each strain.

2001; Le et al., 2013; Yehl et al., 2019) and P2-like phages, while exhibiting strikingly similar structural genes even when infecting different species, have been suggested to coevolve with their bacterial hosts (Nilsson and Haggård-Ljungquist, 2007).

All in all, 52 variable genetic loci were identified among the sequenced clones but none was located inside prophage PP4 sequence (Figure 4 and Supplementary Table S2; Bruneaux et al. (2021)). It can thus be reasonably expected that mutations elsewhere in the genome or epigenetic modifications should be responsible for differences in prophage induction rates and bacteria virulence. To identify the molecular basis of those phenotypic changes, we investigated the association between phenotypic traits and genetic variants present in at least two strains using Wilcoxon rank sum tests adjusted for false-discovery rate (Benjamini and Hochberg, 1995). We also used the methylation data obtained from PacBio SMRT sequencing to test for association between phenotypic traits and adenosine methylation in GATC motifs (which are recognized by an adenine methyltransferase in *S. marcescens*; Ostendorf et al. (1999); Bruneaux et al. (2021)). The main results are summarized below while some details are provided in the Supplementary Results section.

Several of the variable genetic loci associated with prophage induction and bacteria virulence pointed towards a potential role of changes in the biofilm structure and in the outer structure of the cellular envelope in modulating phage particle production and virulence in the insect host (e.g. genes involved in peptidoglycan and LPS biosynthesis, Figure 5 and Supplementary Table S2). Another striking pattern was the presence of three distinct mutations occurring in a single glycosyltransferase gene and close to the putative active site of the protein (mutations *28*, *29* and *30*, Supplementary Figure S5, Supplementary Table S2). These mutations were observed independently in three strains evolved at 24-38 °C and in one strain evolved at 38 °C (which had low prophage induction rates and low virulence compared to the other strains evolved at 38 °C) and support the importance of the outer cellular envelope in the evolutionary response against phages.

Figure 6: (Legend on the next page.)

Figure 6: (Figure on the previous page) Association between phenotypic traits and adenine methylation changes. The heatmap shows Spearman's ρ between methylated fractions of variable m6A epiloci (rows) and phenotypes (columns; Ph., phage release; Vir., bacteria virulence in waxmoth larvae). Overlapping or closest ($\leq$ 500 bp) downstream genes were assigned to each m6A epiloci. Probable gene functions were assigned to each gene product based on a manual literature search. Visualization of the relationship between m6A methylated fractions and phenotypic trait values is shown for the heatmap cells marked with a letter. The m6A epiloci used here were the variable m6A epiloci with a methylation fraction range ≥ 0.2 across sequenced samples and an uncorrected p-value ≤ 0.005 for Spearman's ρ with at least one phenotypic trait.

The functional annotation of genes associated with phenotypic changes via adenosine methylation changes was manually curated based on literature. Many associated genes were involved in functional categories that are critical for pathogen virulence in other bacteria species, such as nutrient capture (important in the challenging host medium; Ren et al. (2018); Liu et al. (2017)), excretion into the outer medium, biofilm formation, adherence, and motility, which all have a key role in colonization and successful invasion of the host tissues (Turner et al., 2009; Luo et al., 2017) (Figure 6). The numerous candidate genes involved in lipopolysaccharide biosynthesis also suggested that the O antigen, which is typically involved both in cell recognition by phages and in bacteria virulence in their host (Chart et al., 1989; Li and Wang, 2012), could act as a major player in evolutionary trade-offs between bacterial virulence and resistance to phage infection. It has been noted previously that *S. marcescens* strains exhibit a large diversity of O antigens (Gaston and Pitt, 1989), and one particular study showed that *S. marcescens* cells grown at different temperatures had different LPS structure and phage affinity, with cells grown at 37 °C having shorter O antigen and lower affinity for LPS-specific phages than cells grown at 30 °C (Poole and Braun, 1988).

Overall, a striking feature of the genetic and epigenetic changes observed in our study was that none of the associated genes was directly connected with thermal selection pressure, which was the primary selective pressure in the evolution experiment, while there was evidence that prophage induction was important in shaping the evolutionary trajectories. For instance, we did not find indication of changes related to

HSP/DNAK genes, even though they are known to be the target of selection in hot and fluctuating environments (Sørensen et al., 2003; Ketola et al., 2004; Sørensen et al., 2016). Such a weak direct effect of the experimentally manipulated factor underlined the fact that indirect selection due to prophage induction overruled the direct effects of temperature.

Conclusion

The cascading effects of abiotic changes observed across a multilevel host-pathogen system caused by evolutionary adaptation of a bacteria to its prophage, with indirect consequences on the bacteria virulence in an insect host, is a novel finding. As bacteria have a strong impact on the biosphere and biochemical cycles, and furthermore can act as important pathogens, the prophages prevalent in bacterial species can indirectly play a major role in global ecological communities and in human health. For instance, the seasonality of prophage induction is related to bacterial and primary production in marine communities (Williamson et al., 2002; Brum et al., 2016), and prophages can affect health through impacts on gut microbiota or by setting the divide between life and death of bacteria's hosts via changes in virulence (Abedon and LeJeune, 2005). Our results provide one clear example of how species interactions can drive the evolutionary response of complex biological systems to abiotic environmental changes. Such a result warrants attention, as a cautionary example of the dangers of considering only single species in isolation and ignoring complex biotic interactions when predicting range expansions and climate change effects on biota.

Materials and Methods

Origin of the strains used in this study

The reference strain was *Serratia marcescens* ATCC 13880. The evolution experiment was performed in an earlier study (Ketola et al., 2013) and is explained briefly here. To initiate the experiment a freshly isolated *Serratia marcescens* ancestor derived from the ATCC 13880 reference strain was grown overnight at 31 °C in the low-nutrient medium SPL 1% (hay extract) to high density and spread to 30 replicate populations (10 populations per thermal treatment). 400 µL populations were placed under constant 31 °C, constant 38 °C, or daily fluctuating (24-38 °C, mean 31 °C) thermal treatments. Resources (hay extract medium) were renewed daily for 30 days and after the experiment clones were isolated from each of the populations by dilution plating samples to LB agar plates. Clones were grown overnight in hay extract to high density after which samples were frozen to 100-well Bioscreen plate and mixed 1:1 with 80 % glycerol, in randomized order. From those frozen stocks, one clone per replicate population was randomly chosen for sequencing. Since two populations from the constant 38 °C treatment were lost during the experimental evolution, we sequenced 10 clones from constant 31 °C, 10 clones from fluctuating 24-38 °C, and 8 clones from constant 38 °C (Supplementary Figure S2).

DNA extraction, sequencing, and genome annotation

Detailed methods for DNA extraction, sequencing with the PacBio SMRT approach, and genome annotation are reported in a companion study (Bruneaux et al., 2021) but a brief overview is given here. The reference strain and randomly selected clones (n = 10, 8 and 10 from 31 °C, 38 °C and fluctuating 24-38 °C evolutionary treatments, respectively) were grown from frozen stocks in overnight precultures followed by 24 h growth in 150 ml of SPL 1%. Bacterial DNA was extracted from pelleted cells and sent for sequencing at the DNA Sequencing and Genomics Laboratory of the University of

Helsinki on a PacBio RS II sequencing platform using P6-C4 chemistry, with two single-molecule real-time sequencing (SMRT) cells run per DNA sample. Standard PacBio analysis protocols were used to assemble genomes and to estimate methylation fractions for adenine bases. Genome annotation was performed using the NCBI Prokaryotic Genome Annotation Pipeline (PGAP; Tatusova et al. (2016)).

Identification of prophage candidates and related sequences

Detection and annotation of prophage candidates

We used the PHASTER prediction tool (Arndt et al., 2016) (https://phaster.ca/) to detect the presence of prophage candidates in the genome of the *Serratia marescens* reference strain we used and sequenced. The submission to the PHASTER server was done on 2019-04-21 and five putative prophages were detected (Supplementary Table S1). Since the candidate prophage PP4 was the only one for which induction was detected in our preliminary assays, we focused our annotation and comparative analysis efforts on this prophage.

The PHASTER output for PP4 contained a set of contiguous CDS in the *S. marcescens* genome which were related to phage functions. It also provided putative locations of attL/attR attachment sequences but those were located between prophage CDS instead of being at their periphery. We searched for better attL/attR candidates by looking for the longest repeated motif located 3000 bp upstream and downstream of the proposed prophage CDS. We found better candidates for attL/attR which encompassed all the PP4 CDS: the corresponding motif was 20-bp long, compared to the 12-bp long motif found by PHASTER. We defined PP4 as the sequence encompassed by those attL/attR sequences.

Annotation of PP4 CDS was manually curated by merging the annotation obtained for the *S. marcescens* genome (as described above) and the annotation provided by PHASTER. A last attempt to identify the CDS for which the "hypothetical protein" status remained at this stage was performed by blasting their predicted protein se-

quences against the nr database using NCBI blastx server and its default settings, but excluding the *Serratia* taxid (blast run on 2020-04-10).

Identification of phages and prophages related to PP4

To identify phages related to PP4, we retrieved all the phage genomes available from RefSeq Nucleotides using the query `Viruses[Organism] AND srcdb_refseq[PROP] NOT wgs[PROP] NOT cellular organisms[ORGN] NOT AC_000001:AC_999999[PACC] AND ("vhost bacteria"[Filter])`. The database was searched on 2020-04-01 and returned 2522 phage genomes. The nucleotide sequence of PP4 was compared to those phage genomes using a local blastn search (task blastn). The three phage genomes giving the total best scores were temperate phages: P88 which infects *Escherichia coli* (KP063541) (Chen et al., 2017) and SEN4 and SEN5 which infect *Salmonella enterica* (KT630645 and KT630646) (Mikalová et al., 2017).

To identify bacterial genomes containing prophages related to PP4, we ran a blastn search of the nucleotide sequence of PP4 against the NCBI nt database (excluding *Serratia* taxid) on 2020-04-02. The bacteria genomes giving the best total scores were *Klebsiella oxytoca* KONIH1 (CP008788.1) and *K. oxytoca* KONIH4 (CP026269.1), which gave very similar scores. We selected KONIH1 for further analysis. To determine the precise locations of PP4-related prophages in the chromosome of KONIH1, we ran a local tblastx search of its sequence against PP4 and produced a dot-plot using the tblastx matches. We visually identified three segments showing a consistent matching structure with PP4. For each segment, we determined the best attL/attR candidates using the same approach used when refining the attL/attR sites for PP4 as described above. This enabled us to extract three prophages (KONIH1/1-3). For each of these prophages, we extracted the CDS contained between their attL/attR based on their GenBank record. Finally, we also searched the genome of the *Serratia* strain we used in our study for other prophages similar to PP4, using the same local tblastx approach as described for KONIH1. The dot plot showed that PP7 was related to PP4, and we

included PP7 in our final comparisons.

Once we extracted the nucleotide sequences for phages P88, SEN4, KSP20 (two fragments available: AB452988.1 and AB452989.1) and for prophages KONIH1/1-3 and PP7, we identified the matches between their predicted proteins and those from PP4 by running a final local tblastx search of each of those sequences against the PP4 sequence.

Quantification of prophage induction using qPCR

Induction rates of the seven candidate prophages (i.e. all prophage regions identified by PHAST, irrespective of the prediction for prophage completeness) were tested under five temperature assay conditions. The assays lasted two days, and were made in SPL 1 % under one of the following treatments: 31-31 °C, 24-24 °C, 38-38 °C, 24-38 °C and 38-24 °C, where the temperatures are the temperatures on the first and second day, respectively, with a transfer to fresh medium between them (Supplementary Figure S6). The details of the induction quantification method are given in the Supplementary Methods, but a brief description is given below.

We used seven specific primer pairs targetting each of the candidate prophage regions and one additional primer pair targetting a chromosomal, non-prophage-related bacterial gene (Supplementary Table S3) to quantify the amount of prophage DNA copies relative to the amount of bacterial genome copies present in a culture using qPCR. The principle of our method is that an excess of prophage DNA copies would indicate prophage induction, as the transition to phage lytic life cycle results in replication of the phage genome, which is followed by assembly of phage progeny and ultimately the lysis of the host cell and the release of phage particles into the medium. Given the low expected induction rates and that for qPCR estimates uncertainty is measured on a logarithmic scale, our approach to reliably quantify the excess of prophage DNA, which might be attributable to prophage induction and released into phage particles, was the following (Supplementary Figure S6): (i) split each culture sample to be analysed into

one raw sample and one supernatant sample obtained after gentle centrifugation to pellet bacteria cells, (ii) process both samples by DNase to digest DNA fragments which were not protected inside a bacterial cell nor inside a phage particle, (iii) inactivate DNase and release DNA from cells and phage particles by heating the samples at 95 °C and (iv) quantify the amount of bacterial genome copies and of prophage DNA copies in both samples with qPCR. The supernatant sample is expected to be impoverished in bacterial cells, while phage particles can remain in suspension, and thus the proportion of prophage DNA copies which were not contained in bacteria cells in the culture (i.e. which were presumably in phage particles) can be estimated from the differential decrease in qPCR estimates for prophage DNA copies and bacteria genome copies between the raw and supernatant samples (see the Supplementary Methods for details of the Bayesian model used to estimate phage-to-bacteria ratios and the effects of assay and evolutionary treatments).

Detection of phage particles by other methods

Transmission electron microscopy

Two precultures of the *S. marcescens* reference strain were grown overnight at 31 °C in 10 ml of SPL 1 % and used to inoculate two volumes of 100 ml of SPL 1 %. After 10 hours, the 100 ml cultures were each added to 300 ml of fresh medium and culture continued for 17 hours at 31 °C. Cells from the two 400 ml batches were pelleted separately (20 min at 8000 rpm with Sorvall RC-6+ centrifuge and F12-6x500 rotor) and their supernatants were filtered with 0.45 µm filters. The filtered supernatant from one 400 ml batch was then pelleted (1.5 hour at 24 000 rpm at 4 °C with Beckman Coulter L-90K centrifuge and 45 Ti rotor) and supernatant was discarded. The filtered supernatant from the second 400 ml batch was added, and a second centrifugation (1.5 hour at 24 000 rpm) was applied. Pellets were resuspended in 1 ml of 0.1 M ammonium acetate and combined. After a last round of centrifugation with the same settings, the final pellet was resuspended in a total of 100 µl of 0.2 M Tris-HCl and stored at 4 °C

until staining for TEM. For staining, 1:10 dilutions of pellet (10 µl) were placed for 1 minute on glow discharge-treated copper grids. Staining was done with 1 % phosphotungstic acid (PTA) for 2 minutes. Imaging was performed with JEOL JEM-1400HC at 80 kV. The resuspended pellet was also used in qPCR reactions similar to the ones used to quantify prophage induction, using all the candidate prophage-specific primers, to confirm the identity of the phage particles observed in TEM.

Plaque assays

The *S. marcescens* reference strain was grown in liquid medium at room temperature and at 37 °C. Supernatants and cells were prepared from both growth conditions. Bacteria (100 µl) were spread on top of 1 % agar plates and the double layer agar method was also employed by mixing 300 µl with 3 ml of 0.7 % soft agar and poured on top of the solid agar. Supernatants (10 µl drops) were applied on plate cultures of the *S. marcescens* reference strain itself, of two freshwater *Serratia* strains, and of Db10 and Db11 *Serratia* strains grown at room temperature and at 37 °C. No plaque was observed for any combination of growth condition of the reference strain with any receiving plate. Additionally, a separate experiment where mitomycin C was added (1 µg ml^{-1}) to liquid cultures of the *S. marcescens* reference strain either at room temperature or at 37 °C did not result in any visible clearing.

Virulence experiment using waxmoth larvae

We estimated the virulence of the experimental strains by measuring the longevity of waxmoth larvae (*Galleria mellonella*) injected with 5 µl of bacterial culture. Bacterial cultures of evolved strains were grown overnight at 31 °C in Bioscreen wells in 400 µl of SPL 1 % inoculated with the strains frozen stocks using a cryoreplicator. The reference strain was similarly grown overnight at 31 °C in 8 ml of SPL 1 % in a loose-capped 15 ml tube inoculated from a frozen sample. On injection day, culture optical densities were measured and each larva was injected with 5 µl of a single culture in the hemocoel

with a Hamilton syringe. For each strain, 20 larvae were injected simultaneously; ten of those were then incubated at 24 °C while the other ten were incubated at 31 °C. Larva survival was monitored at 1-3 hour intervals by checking for larva movements, and time of death was recorded as the inspection time when a larva was found dead. Additionally, for each incubation temperature, ten larvae were injected with sterile medium and ten with sterile water as controls. This setup was replicated four times, resulting in a total of 80 infected larvae per strain (40 to incubation at 24 °C and 40 to incubation at 31 °C). Some larvae from the first replication block were discarded due to a technical problem, leaving three replication blocks instead of four for some strains.

We analysed the larva survival data using a Cox proportional hazards model, where replication block, larval body mass, culture optical density, strain identity, incubation temperature and the interaction between strain identity and incubation temperature were included as fixed effects. In this type of model, the hazard function describes the instantaneous rate of death at a given time t for an individual still alive at t. The model included the effect of strain evolutionary treatment on their virulence, using a hierarchical Bayesian approach in JAGS 4.1.0 (Plummer et al., 2003; Su and Yajima, 2015) with the R2jags package. The proportional hazards were implemented as described by Clayton 1991 (Clayton, 1991) based on code from the OpenBUGS Examples (The OpenBUGS Project). The details of the model are presented in the Supplementary Methods.

Analysis of genetic variation

Since no evidence of genetic polymorphism was found within each sequenced sample, the chromosome sequences of the 29 sequenced strains were simply aligned using Mugsy (Angiuoli and Salzberg, 2011). Variable loci were identified using a custom Python script to identify variable positions in the alignment and to extract allelic information for each sequenced strain. To investigate the association between genetic variation and phenotypic traits, we ran Wilcoxon rank sum tests for all combinations of genetic

variants and phenotypic traits (using only genetic variants present in at least two strains). P-values were corrected for multiple testing using the false-discovery rate method (Benjamini and Hochberg, 1995).

Analysis of epigenetic variation

Epigenetic data consisted of the methylation fraction for adenosine bases in all GATC motifs present in the reference strain genome (38 150 GATC palindromes were present in the reference strain genome, corresponding to 76 300 adenosine bases for which methylation fraction values were analysed). Since the vast majority of the adenosines present in GATC motifs were fully methylated in all sequenced strains, we first selected the subset of GATC motifs which exhibited low methylation level in at least one strain, as decribed in Bruneaux et al. (2021). After this step, 483 palindromes corresponding to 966 adenosines were kept for association analysis with phenotypes (1.2% of all the adenosines in GATC motifs). The significance of the association between each of these 966 epiloci and a given phenotypic trait was calculated as the p-value for Spearman's ρ correlation cofficient between the phenotype values and the m6A methylation fractions for the 29 sequenced strains. We used Spearman's ρ (i.e. rank correlation) to avoid excessive leverage from extreme phenotypic values.

Epiloci were then associated with annotated genes: a gene was assigned to an epilocus if the adenosine base was located within the gene coding region, or less than 500 base pairs upstream of the initiation codon in order to cover potential regulatory regions of the gene. Several gene set approaches were then tested to try to detect biological functions or pathways related to the epiloci associated with phenotypic traits. We used gene-ontology enrichment tests as implemented in the TopGO R package and KEGG pathway analysis with Wilcoxon rank-sum statistics to compare gene sets, but mostly only very general biological functions were detected with those approaches, such as amino acid or carbon metabolism, nutrient transport and translation (data not shown). Since those approaches are targetting the detection of changes affecting a

given biological function or pathway on average, but are not efficient to detect single genes which might affect phenotype, we decided to generate lists of top candidate genes associated with each phenotypic trait (using uncorrected p-value< 0.005 for Spearman's ρ correlation as the threshold) and to manually curate those genes. Manual curation entailed a literature search to provide a brief description of the function of the gene product in bacterial species and to flag genes potentially involved in chosen categories of interest: regulation of transcription, nutrient transport, excretion, cell wall structure, virulence and a larger last category embracing motility, biofilm formation, adherence and quorum sensing. Top candidate genes were then compared across phenotypic traits using a heatmap approach, as shown in Figure 6.

Acknowledgements. We acknowledge Kati Saarinen and Lauri Mikonranta for help with the virulence experiments, Lotta-Riina Sundberg and Leena Lindström for comments on the manuscript, the Academy of Finland (Project 278751) and the Centre of Excellence in Biological Interactions for funding and facilities and the CSC – IT Center for Science, Finland, for computational resources used in this project.

Conflict of interest. The authors declare no competing financial interests.

Authors contributions. TK, JAG and IK conceptualized the study. Experimental design for PacBio sequencing was done by TK and MB. DNA extraction for PacBio sequencing was done by RA. AMÖO identified prophage sequences. AMÖO, RA and MB designed the prophage induction assays and RA and MB performed the assay experiments. EL performed the electron microscopy experiments and the plaque assays and helped analyze PP4 sequence. ZC performed virulence experiments of the sequenced clones in the insect host. RA, IK, MB, and TK performed virulence experiments for the larger pool of evolved clones. MKS assisted with laboratory experiments. MB and IK analysed the sequencing data. MB, IK and TK wrote the original draft with later edits and reviews by all co-authors.

Data availability. PacBio sequencing data (HDF5 files) were submitted to the European Nucleotide Archive's Sequence Read Archive (ENA-SRA, https://www.ebi.ac.uk/ena, project PRJEB40306) and assembled genomes were submitted to NCBI's GenBank (biosamples SAMEA7301478 to SAMEA7301506). Genetic, epigenetic and phenotypic datasets used for analysis will be submitted to the Dryad repository (https://datadryad.org/stash).

Availability of biological materials. The evolved clones of *Serratia marcescens* used in this study are available from the authors upon request.

References

Abedon ST LeJeune JT. 2005. Why Bacteriophage Encode Exotoxins and other Virulence Factors. *Evolutionary Bioinformatics*. 1:117693430500100001.

Angiuoli SV Salzberg SL. 2011. Mugsy: fast multiple alignment of closely related whole genomes. *Bioinformatics*. 27(3):334–342.

Arndt D, Grant JR, Marcu A, Sajed T, Pon A, Liang Y, Wishart DS. 2016. PHASTER: a better, faster version of the PHAST phage search tool. *Nucleic Acids Research*. 44 (W1):W16–W21.

Benjamini Y Hochberg Y. 1995. Controlling the False Discovery Rate: A Practical and Powerful Approach to Multiple Testing. *Journal of the Royal Statistical Society. Series B (Methodological)*. 57(1):289–300.

Brum JR, Hurwitz BL, Schofield O, Ducklow HW, Sullivan MB. 2016. Seasonal time bombs: dominant temperate viruses affect Southern Ocean microbial dynamics. *The ISME Journal*. 10(2):437–449. Number: 2 Publisher: Nature Publishing Group.

Bruneaux M, Kronholm I, Ashrafi R, Ketola T. 2021. Roles of adenine methylation and genetic mutations in adaptation to different temperatures in *Serratia marcescens*. *Epigenetics*. 0(0):1–21.

Buck JC Ripple WJ. 2017. Infectious Agents Trigger Trophic Cascades. *Trends in Ecology & Evolution*. 32(9):681–694.

Canchaya C, Proux C, Fournous G, Bruttin A, Brüssow H. 2003. Prophage Genomics. *Microbiology and Molecular Biology Reviews*. 67(2):238–276.

Casadesús J Low DA. 2006. Epigenetic Gene Regulation in the Bacterial World. *Microbiology and Molecular Biology Reviews*. 70(3):830–856.

Casadesús J Low DA. 2013. Programmed Heterogeneity: Epigenetic Mechanisms in Bacteria. *Journal of Biological Chemistry*. 288(20):13929–13935.

Chart H, Row B, Threlfall EJ, Ward LR. 1989. Conversion of Salmonella enteritidis phage type 4 to phage type 7 involves loss of lipopolysaccharide with concomitant loss of virulence. *FEMS Microbiology Letters*. 60(1):37–40.

Chen M, Zhang L, Xin S, Yao H, Lu C, Zhang W. 2017. Inducible Prophage Mutant of Escherichia coli Can Lyse New Host and the Key Sites of Receptor Recognition Identification. *Frontiers in Microbiology*. 8.

Chevin LM, Lande R, Mace GM. 2010. Adaptation, Plasticity, and Extinction in a Changing Environment: Towards a Predictive Theory. *PLOS Biology*. 8(4):e1000357.

Christie GE Calendar R. 2016. Bacteriophage P2. *Bacteriophage*. 6(1).

Clayton DG. 1991. A Monte Carlo Method for Bayesian Inference in Frailty Models. *Biometrics*. 47(2):467–485.

Flyg C, Kenne K, Boman HG. 1980. Insect pathogenic properties of Serratia marcescens: phage-resistant mutants with a decreased resistance to Cecropia immunity and a decreased virulence to Drosophila. *Journal of General Microbiology*. 120(1): 173–181.

Fortier LC Sekulovic O. 2013. Importance of prophages to evolution and virulence of bacterial pathogens. *Virulence*. 4(5):354–365.

Gaston MA Pitt TL. 1989. Improved O-serotyping method for Serratia marcescens. *Journal of Clinical Microbiology*. 27(12):2702–2705.

Gomez-Gonzalez PJ, Andreu N, Phelan JE, de Sessions PF, Glynn JR, Crampin AC, Campino S, Butcher PD, Hibberd ML, Clark TG. 2019. An integrated whole genome analysis of Mycobacterium tuberculosis reveals insights into relationship between its genome, transcriptome and methylome. *Scientific Reports*. 9(1):5204.

Grimont F Grimont PAD. The Genus Serratia. In Dworkin M, Falkow S, Rosenberg E, Schleifer KH, Stackebrandt E, editors, *The Prokaryotes: Volume 6: Proteobacteria: Gamma Subclass*, pages 219–244. Springer New York, New York, NY, 2006. ISBN 978-0-387-30746-6. doi: 10.1007/0-387-30746-X_11.

Howard-Varona C, Hargreaves KR, Abedon ST, Sullivan MB. 2017. Lysogeny in nature: mechanisms, impact and ecology of temperate phages. *The ISME Journal*.

Kelley LA, Mezulis S, Yates CM, Wass MN, Sternberg MJE. 2015. The Phyre2 web portal for protein modeling, prediction and analysis. *Nature Protocols*. 10(6):845–858.

Ketola T, Mikonranta L, Zhang J, Saarinen K, Örmälä AM, Friman VP, Mappes J, Laakso J. 2013. Fluctuating temperature leads to evolution of thermal generalism and preadaptation to novel environments. *Evolution*. 67:2936–2944.

Ketola T, Laakso J, Kaitala V, Airaksinen S. 2004. Evolution of Hsp90 Expression in Tetrahymena Thermophila (protozoa, Ciliata) Populations Exposed to Thermally Variable Environments. *Evolution*. 58(4):741–748.

Koskella B Brockhurst MA. 2014. Bacteria–phage coevolution as a driver of ecological and evolutionary processes in microbial communities. *Fems Microbiology Reviews*. 38(5):916–931.

Kristensen TN, Ketola T, Kronholm I. 2020. Adaptation to environmental stress at different timescales. *Annals of the New York Academy of Sciences*. 1476(1):5–22. _eprint: https://onlinelibrary.wiley.com/doi/pdf/10.1111/nyas.13974.

Krypotou E, Scortti M, Grundström C, Oelker M, Luisi BF, Sauer-Eriksson AE, Vázquez-Boland J. 2019. Control of Bacterial Virulence through the Peptide Signature of the Habitat. *Cell Reports*. 26(7):1815–1827.e5.

Lamont I, Brumby AM, Egan JB. 1989. UV induction of coliphage 186: prophage induction as an SOS function. *Proceedings of the National Academy of Sciences of the United States of America*. 86(14):5492–5496.

Le S, He X, Tan Y, Huang G, Zhang L, Lux R, Shi W, Hu F. 2013. Mapping the Tail Fiber as the Receptor Binding Protein Responsible for Differential Host Specificity of Pseudomonas aeruginosa Bacteriophages PaP1 and JG004. *PLoS ONE*. 8(7).

Li J Wang N. 2012. The gpsX gene encoding a glycosyltransferase is important for polysaccharide production and required for full virulence in Xanthomonas citri subsp. citri. *BMC Microbiology*. 12(1):31.

Liu W, Huang L, Su Y, Qin Y, Zhao L, Yan Q. 2017. Contributions of the oligopeptide permeases in multistep of Vibrio alginolyticus pathogenesis. *MicrobiologyOpen*. 6 (5).

Luo M, Yang S, Li X, Liu P, Xue J, Zhou X, Su K, Xu X, Qing Y, Qiu J, Li Y. 2017. The KP1_4563 gene is regulated by the cAMP receptor protein and controls type 3 fimbrial function in Klebsiella pneumoniae NTUH-K2044. *PLoS ONE*. 12(7).

López-Garrido J, Puerta-Fernández E, Cota I, Casadesús J. 2015. Virulence Gene Regulation by l-Arabinose in Salmonella enterica. *Genetics*. 200(3):807–819.

Matsushita K, Uchiyama J, Kato Si, Ujihara T, Hoshiba H, Sugihara S, Muraoka A, Wakiguchi H, Matsuzaki S. 2009. Morphological and genetic analysis of three bacteriophages of Serratia marcescens isolated from environmental water. *FEMS Microbiology Letters*. 291(2):201–208.

Mikalová L, Bosák J, Hříbková H, Dědičová D, Benada O, Šmarda J, Šmajs D. 2017. Novel Temperate Phages of Salmonella enterica subsp. salamae and subsp. diarizonae and Their Activity against Pathogenic S. enterica subsp. enterica Isolates. *PLoS ONE*. 12(1).

Nilsson AS Haggård-Ljungquist E. 2007. Evolution of P2-like phages and their impact on bacterial evolution. *Research in Microbiology*. 158(4):311–317.

Ostendorf T, Cherepanov P, Vries Jd, Wackernagel W. 1999. Characterization of a dam Mutant ofSerratia marcescens and Nucleotide Sequence of thedam Region. *Journal of Bacteriology*. 181(13):3880–3885.

Parsonage D, Newton GL, Holder RC, Wallace BD, Paige C, Hamilton CJ, Dos Santos PC, Redinbo MR, Reid SD, Claiborne A. 2010. Characterization of the N-Acetyl-α-d-glucosaminyl l-Malate Synthase and Deacetylase Functions for Bacillithiol Biosynthesis in Bacillus anthracis,. *Biochemistry*. 49(38):8398–8414.

Petersen LM Tisa LS. 2012. Influence of Temperature on the Physiology and Virulence of the Insect Pathogen Serratia sp. Strain SCBI. *Applied and Environmental Microbiology*. 78(24):8840–8844.

Plummer M et al. Jags: A program for analysis of bayesian graphical models using gibbs sampling. In *Proceedings of the 3rd international workshop on distributed statistical computing*, volume 124, page 10. Vienna, Austria., 2003.

Poole K Braun V. 1988. Influence of growth temperature and lipopolysaccharide on hemolytic activity of Serratia marcescens. *Journal of Bacteriology*. 170(11):5146–5152.

Ren W, Rajendran R, Zhao Y, Tan B, Wu G, Bazer FW, Zhu G, Peng Y, Huang X, Deng J, Yin Y. 2018. Amino Acids As Mediators of Metabolic Cross Talk between Host and Pathogen. *Frontiers in Immunology*. 9.

Riva A, Delorme MO, Chevalier T, Guilhot N, Hénaut C, Hénaut A. 2004a. Characterization of the GATC regulatory network in E. coli. *BMC genomics*. 5(1):48.

Riva A, Delorme MO, Chevalier T, Guilhot N, Hénaut C, Hénaut A. 2004b. The difficult interpretation of transcriptome data: the case of the GATC regulatory network. *Computational Biology and Chemistry*. 28(2):109–118.

Scholl D, Rogers S, Adhya S, Merril CR. 2001. Bacteriophage K1-5 Encodes Two Different Tail Fiber Proteins, Allowing It To Infect and Replicate on both K1 and K5 Strains of Escherichia coli. *Journal of Virology*. 75(6):2509–2515. Publisher: American Society for Microbiology Journals Section: RECOMBINATION AND EVOLUTION.

Su YS Yajima M. R2jags: Using R to Run 'JAGS', 2015. R package version 0.5-7.

Suttle CA. 2005. Viruses in the sea. *Nature*. 437(7057):356–361. Number: 7057 Publisher: Nature Publishing Group.

Sørensen JG, Kristensen TN, Loeschcke V. 2003. The evolutionary and ecological role of heat shock proteins. *Ecology Letters*. 6(11):1025–1037.

Sørensen JG, Schou MF, Kristensen TN, Loeschcke V. 2016. Thermal fluctuations affect the transcriptome through mechanisms independent of average temperature. *Scientific Reports*. 6:30975.

Tatusova T, DiCuccio M, Badretdin A, Chetvernin V, Nawrocki EP, Zaslavsky L, Lomsadze A, Pruitt KD, Borodovsky M, Ostell J. 2016. NCBI prokaryotic genome annotation pipeline. *Nucleic Acids Research*. 44(14):6614–6624.

The OpenBUGS Project. Leuk: survival analysis using Cox regression.

Turner KH, Vallet-Gely I, Dove SL. 2009. Epigenetic Control of Virulence Gene Expression in Pseudomonas aeruginosa by a LysR-Type Transcription Regulator. *PLoS Genetics*. 5(12):e1000779.

Williamson SJ, Houchin LA, McDaniel L, Paul JH. 2002. Seasonal Variation in Lysogeny as Depicted by Prophage Induction in Tampa Bay, Florida. *Applied and Environmental Microbiology*. 68(9):4307–4314.

Yehl K, Lemire S, Yang AC, Ando H, Mimee M, Torres MDT, de la Fuente-Nunez C, Lu TK. 2019. Engineering Phage Host-Range and Suppressing Bacterial Resistance through Phage Tail Fiber Mutagenesis. *Cell*. 179(2):459–469.e9.

Zarnetske PL, Skelly DK, Urban MC. 2012. Biotic Multipliers of Climate Change. *Science*. 336(6088):1516–1518.

Supplementary Results

Association between genetic changes and phenotypic traits

The variable loci most clearly associated with both phage release and bacteria virulence in the insect host were the variant *a* and the pooled variants related to galactokinase (pooled variants *b*, *c*, and *h*) and related to glycosyltransferase (pooled variants *e*, *27*, *28*, and *29*) (Figure 5). These genetic variants were located in or close to ($\leq$ 500 bp) genes annotated as transcriptional regulators (molybdenum-dependent transcriptional regulator and transcriptional regulator RcsB involved in motility and capsule and biofilm formation in *E. coli*) and enzymes involved in the cell wall and outer membrane structure and biofilm formation (peptidoglycan synthase, two glycosyltransferases and a cellulose biosynthesis protein BcsG) (Supplementary Table S2). Those genes point towards a potential role for modifications of biofilm structure and of the outer structure of the cellular envelope in modulating phage particle production and virulence in the insect host. In particular, the three independent mutations located in a single glycosyltransferase gene (mutations *28*, *29* and *30*, close to the putative active site of the protein; Supplementary Figure S5; Supplementary Table S2) were observed independently in several strains: three strains evolved at 24-38 °C and one strain evolved at 38 °C. Those independent mutations point to the important role of the outer cellular envelope in the evolution against phage.

Finally, we also noted that haplotype *a*, comprising eleven associated genetic loci, was shared by 5 out of the 8 strains evolved at 38 °C and by the reference strain, but by none of the other sequenced strains. This points to the probable existence of some standing genetic variation at the onset of the experiment, which was then subjected to selection during the experimental evolution (Bruneaux et al., 2021).

Association between epigenetic changes and phenotypic traits

In addition to nucleotide sequences, the data we obtained from the PacBio SMRT method also provided information about base methylation. In *S. marcescens*, adenosines present in GATC motifs are methylated into m6A by the Dam enzyme at a very high rate (>98% of GATC motifs were methylated on both strands in our dataset; Bruneaux et al. (2021)). The remaining GATC motifs can be either hemi-methylated or unmethylated in a cell, and are often variably methylated across cells of a given culture and across strains. Adenosine methylation can influence gene expression by affecting the binding of regulatory proteins to promoter regions of genes (Gomez-Gonzalez et al., 2019) or by affecting transcription speed via increased DNA stability of gene bodies (Riva et al., 2004a,b). Such epigenetic regulation can be maintained across rounds of DNA replication by competitive binding to target DNA between the Dam responsible for methylation and regulatory proteins specific to the same region (Casadesús and Low, 2006, 2013), and can thus be subject to selection.

Among GATC motifs which were not fully methylated in our dataset, no association was found between evolutionary treatments and methylated fractions (Bruneaux et al., 2021). However, we identified adenosines for which changes in methylation level were associated with phenotypic changes in the traits measured here (phage induction and virulence in an insect host). For a given phenotypic trait, GATC loci exhibit-

ing both positive and negative correlations between methylated fractions and the trait values could be observed (Figure 6, heatmap panel). Manual curation of the function of the genes associated with GATC motifs related to phenotypic changes showed that many of them were involved in (1) transcription regulation, (2) nutrient capture and transport into the cell, (3) excretion into the outer medium, (5) biofilm formation, adherence or motility, and (6) cell envelope structure (including peptidoglycan and lipopolysaccharide biosynthesis) (Figure 6, gene functions panel). Many of those functional categories have been shown to be critical for pathogen virulence in other bacterial species, in particular for nutrient capture in the challenging host medium (Ren et al., 2018; Liu et al., 2017), for recognition of the host habitat via its nutrient signature (López-Garrido et al., 2015; Krypotou et al., 2019) and for biofilm formation, adherence and motility which have a key role in colonization and successful invasion of the host tissues (Turner et al., 2009; Luo et al., 2017). The numerous candidate genes involved in lipopolysaccharide biosynthesis also suggest that the O antigen, which can classically be involved both in cell recognition by phages and in bacterial virulence in its host (Chart et al., 1989; Li and Wang, 2012), could act as a major player of evolutionary trade-offs between bacterial virulence and resistance to phage infection.

Supplementary Methods

Quantification of phage induction using qPCR

Culture conditions for the temperature assays

Frozen stocks had been stored at −80 °C in 40 % glycerol, with evolved clones stored in 100-well plates (Bioscreen measurement plates), in randomized order and reference clone stored in microcentrifuge tubes. A preculture step in 400 µl of SPL 1 % at 31 °C was performed by using a cryo-replicator to inoculate evolved clones into a new 100-well plate and by inoculating the reference strain into wells of another plate. After 24 hours, five identical 100-well assay plates containing both the 28 evolved clones of interest and the reference clone were prepared by transferring 40 µl of each preculture into 360 µl of fresh SPL 1 % (1 well per clone, i.e. 29 wells occupied per plate). For the first day of assay, one plate was incubated at 31 °C, two plates at 24 °C and two plates at 38 °C. After 24 hours, clones within a given plate were transferred to 29 previously empty new wells in the same plate (40 µl culture into 360 µl fresh medium). For the second day of assay, the plate from 31 °C was kept at 31 °C, one plate from 24 °C was kept at 24 °C and the other was transferred to 38 °C, and one plate from 38 °C was kept at 38 °C while the other was transferred to 38 °C. After 24 hours, plates were taken for sample processing. Extra wells containing sterile SPL 1 % medium were used on the assay plates to monitor potential contamination during plate handling (which was not observed). The whole experiment was performed twice, starting with the same frozen stocks but with independent precultures.

Sample processing and qPCR runs

At the end of the second day of assay, each of the 29 cultures in each of the 5 assay plates was processed in the following way: 50 µl of native culture sample was transferred to a 96-well PCR plate, while the rest of the culture was placed into a microcentrifuge tube, centrifuged at 13 500 g for 5 min and 50 µl of supernatant was transferred in the 96-well plate, resulting in two paired samples per culture (native and supernatant). Samples from a given assay plate were placed into the same 96-well plate. A DNase treatment was then performed to digest DNA fragments which were not protected inside a bacteria cell or a phage particle. 5 µl of DNase I at 0.1 mg ml^{-1} were added to each sample, followed by an incubation at 37 °C for 30 min. DNA was then released from bacteria cells and potential phage particles by incubating the samples at 95 °C for 30 min after having added 5 µl of EGTA (20 mM, pH 8) in order to hinder DNase I activity. The sample plates were then stored at −20 °C until DNA quantification by qPCR runs.

Quantification of DNA target sequences was performed using prophage-specific primer pairs and one bacterial-gene-specific primer pair (Supplementary Table S3). Preliminary experiments using the reference strain at 31 °C having showed no detectable extra-cellular DNA at least for prophages 2 and 5, six qPCR were runs per 96-well sample plate from this experiment using primers for prophages 1, 3, 4, 6, 7 and for bacterial gene purA2. Runs were performed using CFX Real Time PCR detection system (Bio-Rad laboratories, USA). Amplifications were performed in a final volume

of 10 µl, containing 5 µl of 2 x IQ SYBR Green Supermix (Bio-Rad), 0.5 µl of forward and reverse primers (6 µM each) and 1 µl of undiluted sample. Amplifications for each primer pair were performed on separate qPCR plates, with in-plate calibration samples for each run. Calibration samples were prepared by serial dilution of a stock solution of purified *Serratia marcescens* DNA of known concentration, and ranged in concentration from 10^6 to 1 genome copy per qPCR well, based on the predicted molecular weight of *S. marcescens* chromosome. Experimental and calibration samples were run in triplicates within each qPCR plate. The qPCR reaction used an initial denaturation step lasting 3 min at 95 °C, followed by 41 cycles consisting of denaturation at 95 °C for 10 s, annealing at 61 °C (for all prophage primers) or 56 °C (for bacterial gene primers) for 10 s, and elongation at 72 °C for 30 s. A melt curve analysis was performed at the end of the run to check the quality of the amplified product (from 65 °C to 95 °C, using increments of 0.5 °C and 5 s steps). In-plate calibration samples were used to estimate the efficiency E of the qPCR reaction with the formula $E = -1 + 10^{(-1/\beta)}$ where β is the slope of the linear relationship between Cq values and $\log_{10}$(concentration) for the calibration samples. To test for an effect of potentially undegraded RNA molecules on phage activation estimates, some samples were incubated with RNase for 30min just prior to qPCR runs. Estimates of phage activation for those samples were similar whether the samples were treated or untreated with RNase prior to qPCR runs, hence data from both RNase-treated and untreated qPCR runs was used for downstream analysis.

Estimation of prophage induction rates and treatment effects using a Bayesian model

We incorporated into a single Bayesian model the simultaneous estimation of phage induction rates and of the effects of assay temperature and evolutionary treatment. To simplify its presentation here, we will first explain the modelling part related to the estimation of induction rates for each culture well, based on the Cq values for the native and supernatant samples obtained from qPCR runs with bacterial and prophage primers, before explaining the incorporation of assay and evolutionary treatment effects.

Let $c_{bact,nat}$ be the number of bacterial chromosome copies present in a native sample. The value of $c_{bact,nat}$ is determined from the qPCR run using the bacterial-gene-specific purA2 primers. Let $c_{pro,nat}$ be the number of prophage DNA copies present in the native sample for e.g. prophage KSP20. The value of $c_{pro,nat}$ is determined from the qPCR run using the prophage-specific primers. Let's assume that this prophage is induced into phage particles at an activation rate a, such that the number of phage particles present in the native sample $c_{phg,nat}$ is related to the number of bacteria cells (i.e. the number of bacteria chromosome copies) by $c_{phg,nat} = a \times c_{bact,nat}$. Since the prophage primers can target the prophage sequence both in the bacterial genome and

in phage particles, we have:

$$c_{pro,nat} = c_{bact,nat} + c_{phg,nat}$$
$$c_{pro,nat} = c_{bact,nat} + a \times c_{bact,nat}$$
$$c_{pro,nat} = (1 + a) \times c_{bact,nat}$$

After centrifugation, we assume most bacteria cells have been pelleted and most phage particles (if any) have remained in suspension. Let k be the concentration factor during centrifugation for this culture, so that $k = (c_{bact,sup}/c_{bact,nat})$ where $c_{bact,sup}$ is the number of bacterial chromosome copies present in the supernatant samples, as determined by qPCR with purA2 primers ($0 \leq k \leq 1$). If $c_{pro,sup}$ is the number of prophage DNA copies in the supernatant sample determined by qPCR with the prophage primers and $c_{phg,sup}$ is the number of phage particles in the supernatant sample, and if we assume $c_{phg,sup} = c_{phg,nat}$ (i.e. we assume that the amount of phage particles pelleted during centrifugation is negligible), we have:

$$c_{pro,sup} = c_{bact,sup} + c_{phg,sup}$$
$$c_{pro,sup} = k \times c_{bact,nat} + c_{phg,nat}$$
$$c_{pro,sup} = k \times c_{bact,nat} + a \times c_{bact,nat}$$
$$c_{pro,sup} = (k + a) \times c_{bact,nat}$$

Thus, to summarize, the two fundamental equations that relate the four qPCR measurements for a given culture ($c_{bact,nat}$ / $c_{bact,sup}$ / $c_{pro,nat}$ / $c_{pro,sup}$) and the prophage activation rate a in this culture are:

$$c_{pro,nat} = (1 + a) \times c_{bact,nat}$$
$$c_{pro,sup} = \left(\frac{c_{bact,sup}}{c_{bact,nat}} + a \right) \times c_{bact,nat}$$

We describe below the integrated Bayesian model used to estimate phage activation rates based on those two equations and on the Cq data obtained from qPCR runs. Note that in the model description below, all parameters corresponding to DNA concentrations are expressed in number of target copies per qPCR well (copies/well).

The model relates Cq values to DNA concentrations, using plate-specific calibration parameters (calibration samples were present in all qPCR plates). Firstly, the model likelihood component due to the calibration samples is (with n_{cal} being the total number

of qPCR wells containing a calibration sample in our dataset):

$$\begin{aligned} \forall i \in \{1 \dots n_{cal}\}, \qquad c_i^{well} &\sim \text{Poisson}(cal_i) \\ \text{Cq}_i^{pred} &= \alpha_{run_i} + \beta_{run_i} \times \log_{10}\left(c_i^{well}\right) \\ \text{Cq}_i^{cal} &\sim \text{normal}(\mu = \text{Cq}_i^{pred}, \sigma = \sigma_{\text{Cq}}) \end{aligned}$$

where cal_i is the expected number of target copies in the well (between 1 and 10^5 in our experiment), c_i^{well} is the actual number of target copies in the well, $\alpha_{[.]}$ and $\beta[.]$ are calibration parameters describing the relationship between Cq values and DNA concentrations, $run_i \in \{1 \dots n_{runs}\}$ is the index of the qPCR plate corresponding to the calibration sample and Cq_i^{cal} is the observed Cq value for the sample. Note that $\alpha_{[.]}$ and $\beta_{[.]}$ are plate-specific (i.e. they are indexed by run_i) to account for plate variability in the qPCR efficiency, while the parameter σ_{Cq} which accounts for the experimental noise in the observed Cq values is shared across all qPCR runs. Note also that we use a Poisson distribution for c_i^{well} to more accurately describe the sampling process happening when pipetting the template from their preparative tubes into the qPCR wells, especially at low template concentrations.

Secondly, we describe the model likelihood component due to the qPCR wells containing the experimental samples of unknown concentrations prepared from the cultures in the assay plates. For this, we set (with n_{unkn} being the number of qPCR wells with samples of unknown concentration and $cult_i$ the index of the original culture for each unknown sample):

$$\forall i \in \{1 \dots n_{unkn}\}, \qquad unkn_i = \begin{cases} c_{bact,nat,cult_i} & \text{or} \\ c_{bact,sup,cult_i} & \text{or} \\ c_{pro,nat,cult_i} & \text{or} \\ c_{pro,sup,cult_i} & \end{cases}$$

depending on whether the unknown sample is run with purA2 ($c_{bact,.,.}$) or prophage ($c_{pro,.,.}$) primers and whether it is native ($c_{.,nat,.}$) or from supernatant ($c_{.,sup,.}$). The likelihood due to unknown samples is then of the same form as for the calibration samples:

$$\begin{aligned} \forall i \in \{1 \dots n_{unkn}\}, \qquad c_i^{well} &\sim \text{Poisson}(unkn_i) \\ \text{Cq}_i^{pred} &= \alpha_{run_i} + \beta_{run_i} \times \log_{10}\left(c_i^{well}\right) \\ \text{Cq}_i^{cal} &\sim \text{normal}(\mu = \text{Cq}_i^{pred}, \sigma = \sigma_{\text{Cq}}) \end{aligned}$$

The remaining deterministic relationships of the model and the priors used for

unknown parameters to estimate are:

$$\forall i \in \{1 \dots n_{runs}\}, \qquad \begin{aligned} \alpha_i &\sim \text{normal}(\mu = 40, \sigma = 10) \\ \beta_i &\sim \text{normal}(\mu = 3.5, \sigma = 2) \\ \sigma_{Cq} &\sim \text{half-Cauchy}(\text{scale} = 2.5) \end{aligned}$$

for the parameters of the qPCR calibration curve for each run (note that σ_{Cq} is shared across all qPCR runs) and:

$$\forall i \in \{1 \dots n_{cultures}\}, \qquad \begin{aligned} \log_{10}(c_{bact,nat,i}) &\sim \text{uniform}(0, 20) \\ \log_{10}(c_{bact,sup,i}) &= \log_{10}(k_i) + \log_{10}(c_{bact,nat,i}) \\ \log_{10}(c_{pro,nat,i}) &= \log_{10}(1 + a_i) + \log_{10}(c_{bact,nat,i}) \\ \log_{10}(c_{pro,sup,i}) &= \log_{10}(k_i + a_i) + \log_{10}(c_{bact,nat,i}) \\ \log_{10}(k_i) &\sim \text{half-Cauchy}(\text{scale} = 2) \\ \log_{10}(a_i) + 4 &\sim \text{gamma}(\mu = 2, \sigma = 2) \end{aligned}$$

for the characteristics of a given culture well. Note that here, we assume that the minimum value of activation rate a is 10^{-4}, which is approximatively the lower sensitivity threshold predicted for our method when we assume that Cq values are measured with a standard deviation $\sigma_{Cq} \approx 0.48$ (Supplementary Figure S7). We model this as $(\log_{10}(a_i) + 4)$ following a Gamma distribution. In this explanation, we use fixed values for the parameters of the Gamma distribution, but when we will introduce the effect of assay and evolutionary treatment the μ and σ parameters of this Gamma distribution will depend on the treatments.

This model formulation is sufficient to obtain posterior distributions for $\log_{10}(a_i)$ for each culture well i in the assay plates. To model the effect of assay and evolutionary treatment, we extend the model by modifying the parameters of the previous prior for a_i:

$$\log_{10}(a_i) + 4 \sim \text{gamma}(\mu = 2, \sigma = 2)$$

by:

$$\forall i \in \{1 \dots n_{cultures}\}, \qquad \begin{aligned} \log_{10}(a_i) + 4 &\sim \text{gamma}(\mu = \mu_i, \sigma = \sigma_i) \\ \mu_i &\sim \exp(\beta_{assay}[assay_i] + \beta_{str}[str_i]) \\ \sigma_i &= \sigma_{assay}[assay_i] \end{aligned}$$

where $assay_i$ is the index of the assay treatment for culture i ($assay_i \in \{1 \dots 5\}$) and str_i is the index of the strain ID for culture i ($str_i \in \{1 \dots 29\}$). The priors for the

effect of assay treatments are:

$$\begin{aligned} \text{Intercept:} \quad & \beta_{assay}[1] = 1 \\ \forall i \in \{2 \dots 5\}, \quad & \beta_{assay}[i] \sim \text{normal}\,(\mu = 0, \sigma = 4) \\ \forall i \in \{1 \dots 5\}, \quad & \sigma_{assay}[i] \sim \text{uniform}(0, 10) \end{aligned}$$

The strain effects include a hierarchical effect of the evolutionary treatment (four levels: three evolution environments plus the reference strain). The priors for the strain and evolutionary treatment effects are:

$$\begin{aligned} \forall i \in \{1 \dots 29\}, \quad & \beta_{str}[i] \sim \text{normal}\,(\mu = \mu_{evo}[evo_i], \sigma = \sigma_{evo}[evo_i]) \\ \forall i \in \{1 \dots 4\}, \quad & \mu_{evo}[i] \sim \text{normal}\,(\mu = 0, \sigma = 4) \\ & \sigma_{evo}[i] \sim \text{uniform}\,(0, 10) \end{aligned}$$

where evo_i is the index of the evolutionary treatment for strain i.

Bayesian implementation of the Cox proportional hazards mixed model

The virulence experiment dataset contained observations for $N = 2182$ individual larvae. For each larvae i, survival time s_i was calculated as the difference between recorded death time and injection time. The survival timeline for all larvae was divided into $T = 20$ intervals, so that the $s_{i,i\in\{1\dots N\}}$ values were homogeneously distributed across intervals (i.e. all intervals contained approximatively the same number of death events). Intervals were defined by their boundaries $t_{j,j\in\{1\dots T+1\}}$, such that interval j is $[t_j, t_{j+1})$ and is of duration $dt_j = t_{j+1} - t_j$.

The survival data was transformed into a risk variable $Y_i(j)$ and an event count variable $dN_i(j)$ defined for all $i \in \{1 \dots N\}$ and $j \in \{1 \dots T\}$ by:

$$Y_i(j) = \begin{cases} 1 & \text{if } s_i > t_j \\ 0 & \text{otherwise} \end{cases} \quad \text{and } dN_i(j) = \begin{cases} 1 & \text{if } s_i \in [t_j, t_{j+1}) \\ 0 & \text{otherwise} \end{cases}$$

The model assumes:

$$dN_i(j) \sim \text{Poisson}(Y_i(j) \times d\lambda_0(j) \times \exp(\beta z_i) \times dt_j)$$

where $d\lambda_0(j)$ is the increment in the integrated baseline hazard from t_j to t_{j+1} and βz_i is the product of the model parameters and of the covariate values for larva i. The term βz_i corresponds to:

$$\begin{aligned} \beta z_i = \quad & \beta_{blk}[blk_i] + \beta_{BM} BM_i + \beta_{OD} OD_i + \beta_{str|incub24}[str_i] \times (1 - incub_i) \\ & + \beta_{str|incub31}[str_i] \times incub_i \end{aligned}$$

where blk_i, BM_i, OD_i, str_i, and $incub_i$ are respectively the replication block, body mass, preculture OD, injected strain ID ($str_i \in \{1 \dots 29\}$) and incubation temperature (0 for

24 °C, 1 for 31 °C) for larva i. Square brackets indicate indexing of a vector parameter; β_{blk} is a vector containing the replication block effects and $\beta_{str|incub24}$ and $\beta_{str|incub31}$ are vectors containing the strain effects in the 24 °C and 31 °C incubations, respectively. To model the effect of the evolutionary treatment, we set, for $k \in \{1 \dots 29\}$:

$$\beta_{str|incub24}[k] \sim \text{normal}\left(\mu_{incub24}[evo[k]], \sigma_{incub24}[evo[k]]\right)$$
$$\beta_{str|incub31}[k] \sim \text{normal}\left(\mu_{incub31}[evo[k]], \sigma_{incub31}[evo[k]]\right)$$

where the vector *evo* allows to map the strain ID and one of the four evolutionary treatments (three different temperature regimes plus reference strain).

The priors we used were:

$$\begin{aligned}
\beta_{blk}[.] &\sim \text{normal}(\text{mean} = 0, \text{sd} = 10) \\
\beta_{BM} &\sim \text{normal}(0, 10) \\
\beta_{OD} &\sim \text{normal}(0, 10) \\
\mu_{incub24}[.] &\sim \text{normal}(0, 2) \\
\mu_{incub31}[.] &\sim \text{normal}(0, 2) \\
\sigma_{incub24}[.] &\sim \text{uniform}(\text{min} = 0, \text{max} = 10) \\
\sigma_{incub31}[.] &\sim \text{uniform}(0, 10)
\end{aligned}$$

and for all $j \in \{1 \dots T\}$:

$$\begin{aligned}
d\lambda_0(j) &\sim \text{gamma}(\text{mean} = d\lambda_0^*(j), \text{rate} = c) \\
d\lambda_0^*(j) &= r \times dt_j
\end{aligned}$$

with $c = 0.001$ and $r = 0.1$. We used the first replication block and the effect of the reference strain in the 24 °C incubation as the references:

$$\begin{aligned}
\beta_{blk}[1] &= 1 \\
\mu_{incub24}[anc] &= 1
\end{aligned}$$

We ran four chains in parallel with the JAGS MCMC sampler for 10 000 iterations per chain, of which the first 5000 were discarded as burn-in. Model convergence and chain mixing was assessed by visual examination of trace plots and calculation of $\hat{R}$ values.

Selection of m6A in non-fully methylated GATC motifs

The method to identify GATC loci which were not fully methylated in our dataset was reported in a companion study (Bruneaux et al., 2021). Briefly, we calculated for each GATC locus the distance between the point defined by its methylated fractions on the plus and minus strand and the point corresponding to full methylation on both strands (1,1). We then defined the set of partially methylated GATC loci of interest as the loci which deviated from the point of full methylation more than four times the average quadratic distance to (1, 1) in at least one sequenced strain.

Supplementary tables

Prophage ID	Position in reference strain genome	Size (kb)	Completeness
PP1	521 990-535 146	13.2	incomplete
PP4 (KSP20-like)	1 970 982-2 003 867	32.9	intact
PP5	3 451 823-3 468 581	16.8	intact
PP6	3 914 469-3 946 913	32.4	incomplete
PP7	4 423 686-4 461 768	34.5	intact

Supplementary Table S1: In-silico detection of prophage sequences in *S. marcescens* reference strain genome. Predictions were run on the PHASTER server on 2019-04-21.

ID	Haplotype	Freq.	Distrib. (31/fl./38)	Pos. (bp)	Type	Region	Effect	Overlapping or closest (≤500bp) gene	
								Name	Function
01	f	1/28	0/1/0	31 753	SNP	CDS	non-syn.	DUF3053 domain-containing protein	unknown
02	a	*5/28	0/0/5	40 239	SNP	CDS	non-syn.	HAP resistance protein	Unknown
03	d	1/28	0/1/0	70 546	indel	CDS	frameshift	Icd-like protein	host cell division inhibitor
04		6/28	2/3/1	92 159	indel	non-CDS	-	-	-
05	b	1/28	0/0/1	108 315	indel	non-CDS	-	PTS beta-glucoside transporter	carbohydrate import
06	a	*5/28	0/0/5	131 841	SNP	CDS	non-syn.	cellulose biosynthesis protein BcsG	biofilm?
07		1/28	1/0/0	173 551	indel	non-CDS	-	protoheme IX biogenesis protein HemY	heme metabolism
08	a	*5/28	0/0/5	328 601	SNP	CDS	non-syn.	condensation protein	non-ribosomal peptide synthesis
09		1/28	0/0/1	391 159	indel	CDS	frameshift	RNA chaperone Hfq	regulation of stress transcription factors
10	g	1/28	1/0/0	429 888	indel	non-CDS	-	transcriptional regulator	similar to regulator of E. coli phage Mu
11		4/28	0/4/0	522 878	indel	CDS	frameshift	integrase	prophage DNA Integration/excision
12	b	1/28	0/0/1	751 961	indel	CDS	frameshift	DNA polymerase II	DNA elongation
13	b	1/28	0/0/1	770 532	indel	non-CDS	-	leu operon leader peptide	leucine biosynthesis
14		1/28	1/0/0	914 534	indel	CDS	frameshift	hydroxyacylglutathione hydrolase	lactate metabolism/response to heat
15		1/28	0/1/0	979 119	indel	non-CDS	-	hypothetical protein	unknown
16	f	1/28	0/1/0	1 093 517	indel	CDS	frameshift	competence protein ComEA	cell surface DNA binding
17		1/28	1/0/0	1 185 019	indel	CDS	frameshift	hypothetical protein	unknown
18	c	1/28	0/0/1	1 311 662	indel	CDS	no frameshift	galactokinase	galactose metabolism
19	b	1/28	0/0/1	1 311 735	SNP	CDS	non-syn.	galactokinase	galactose metabolism
20	h	1/28	0/0/1	1 311 996	SNP	CDS	non-syn.	galactokinase	galactose metabolism
21	a	*5/28	0/0/5	1 317 345	SNP	CDS	syn.	Mo-dependent transcriptional regulator	regulation of transcription
22		5/28	1/2/2	1 421 879	indel	non-CDS	-	acyl carrier protein	Fatty acid/polyketide biosynthesis
23	d	1/28	0/1/0	1 609 697	indel	non-CDS	-	transcriptional regulator GalS	regulation of galactose transport/catabolism
24		1/28	0/0/1	1 610 617	indel	CDS	frameshift	galactose/galactoside ABC transporter MglB	galactose import
25		1/28	0/1/0	1 611 529	SNP	CDS	non-syn.	galactose/galactoside ABC transporter MglA	galactose import
26		1/28	1/0/0	1 612 777	indel	CDS	no frameshift	galactose/galactoside ABC transporter MglC	galactose import
27		4/28	0/3/1	1 665 941	indel	CDS	frameshift	glycosyltransferase	LPS biosynthesis
28		1/28	0/1/0	1 670 147	SNP	CDS	non-syn.	glycosyltransferase	LPS biosynthesis
29		2/28	0/1/1	1 670 356	SNP	CDS	non-syn.	glycosyltransferase	LPS biosynthesis
30	e	1/28	0/1/0	1 670 370	SNP	CDS	non-syn.	glycosyltransferase	LPS biosynthesis
31	a	*5/28	0/0/5	1 861 227	indel	non-CDS	-	putative transcriptional regulator	regulation of transcription
32		1/28	0/0/1	2 144 682	indel	non-CDS	-	hypothetical protein	unknown

(Continued on next page.)

ID	Haplotype	Freq.	Distrib. (31/fl./38)	Pos. (bp)	Type	Region	Effect	Overlapping or closest (≤500bp) gene	
								Name	Function
33		1/28	0/1/0	2 282 483	indel	non-CDS	-	MATE family efflux transporter	Na+/H+ driven multidrug efflux pump
34	h	1/28	0/0/1	2 353 326	indel	CDS	frameshift	fumarase C (iron independent)	TCA cycle
35	b	1/28	0/0/1	2 384 093	indel	CDS	frameshift	HlyD (haemolysin secretion system)	haemolysin/cutinase excretion
36	a	*5/28	0/0/5	2 456 338	SNP	CDS	non-syn.	peptidoglycan synthase	peptidoglycan biosynthesis
37		2/28	2/0/0	2 466 586	SNP	CDS	non-syn.	MmgE/PrpD family protein	propionate metabolism/TCA cycle?
38	e	1/28	0/1/0	2 941 884	indel	non-CDS	-	VOC family protein	unknown
39		2/28	2/0/0	3 161 361	SNP	CDS	syn.	serine/threonine protein kinase	regulation of cell processes
40	e	1/28	0/1/0	3 408 594	indel	non-CDS	-	nucleoside diphosphate hydrolase	regulation of cell processes
41	a	*5/28	0/0/5	3 477 366	SNP	CDS	non-syn.	transcriptional regulator RcsB	capsule synthesis/cell division/biofilm/motility
42		*0/28	-	3 600 509	indel	non-CDS	-	phospholipid-binding lipoprotein MlaA	Outer membrane maintenance
43	a	*5/28	0/0/5	3 607 617	SNP	CDS	non-syn.	heme exporter protein CcmB	cytochrome c biogenesis
44	a	*5/28	0/0/5	3 869 219	SNP	CDS	syn.	cytochrome c	energy metabolism
45		1/28	1/0/0	4 025 724	indel	non-CDS	-	acetyl-CoA carboxylase alpha subunit	lipid metabolism
46		1/28	1/0/0	4 337 062	indel	non-CDS	-	tRNA-Phe	translation
47		1/28	0/0/1	4 362 753	indel	non-CDS	-	glycoporin	carbohydrate import
48	c	1/28	0/0/1	4 845 837	indel	CDS	frameshift	peptidylprolyl isomerase	protein folding chaperone
49	g	1/28	1/0/0	4 872 989	indel	CDS	frameshift	short chain dehydrogenase	oxidoreductase
50	d	1/28	0/1/0	4 924 755	SNP	CDS	non-syn.	threonine dehydratase	amino acid metabolism
51	a	*5/28	0/0/5	5 010 850	indel	CDS	frameshift	deacetylase	LPS biosynthesis
52	a	*5/28	0/0/5	5 010 868	SNP	CDS	non-syn.	deacetylase	LPS biosynthesis

Supplementary Table S2: Genetic variants observed in the 29 sequenced clones (from Bruneaux et al. (2021)). Haplotype: letters identify groups of co-occurring mutations. Freq.: minor allele frequency observed among the 28 evolved clones (an asterisk marks loci for which the reference strain carried the minor allele). Distrib.: distribution of minor alleles across the strains evolved in the 31 °C, 24-38 °C and 38 °C treatments.

818

Target	Name	Sequence
Prophage 1	ph1-F	5′-CGGACGTTCTTTCCTCTGCT-3′
	ph1-R	5′-AGCTCTGCAGCGTTATCCAG-3′
Prophage 4 (PP4)	ph4-F	5′-CTTTGGTTCAGGCGTCATGG-3′
	ph4-R	5′-GTAAACCAGTCCCACACGCT-3′
Prophage 5	ph5-F	5′-GCCACATATCCCAGCGTTGA-3′
	ph5-R	5′-ATGGCAAGCCACAGATAGGT-3′
Prophage 6	ph6-F	5′-GTGCCGAAGGAATGGCCTTA-3′
	ph6-R	5′-CTGAAATTGCTTCGCGCCAT-3′
Prophage 7	ph7-F	5′-GTCAAAGGGGTTAAGCTCGC-3′
	ph7-R	5′-GAACAGAACGGCGCACTACA-3′
Bacterial gene	purA2-F	5′-ATGTGGATTACGTGCTGGGC-3′
	purA2-R	5′-CACAGGTATTCGCCGGTTTC-3′

Supplementary Table S3: Sequences of the primers used in the qPCR quantification of prophages and chromosomal DNA. The purA2-F/R primers are targeting the chromosomal, non-prophage-related bacterial gene for adenylosuccinate synthetase.

Supplementary figures

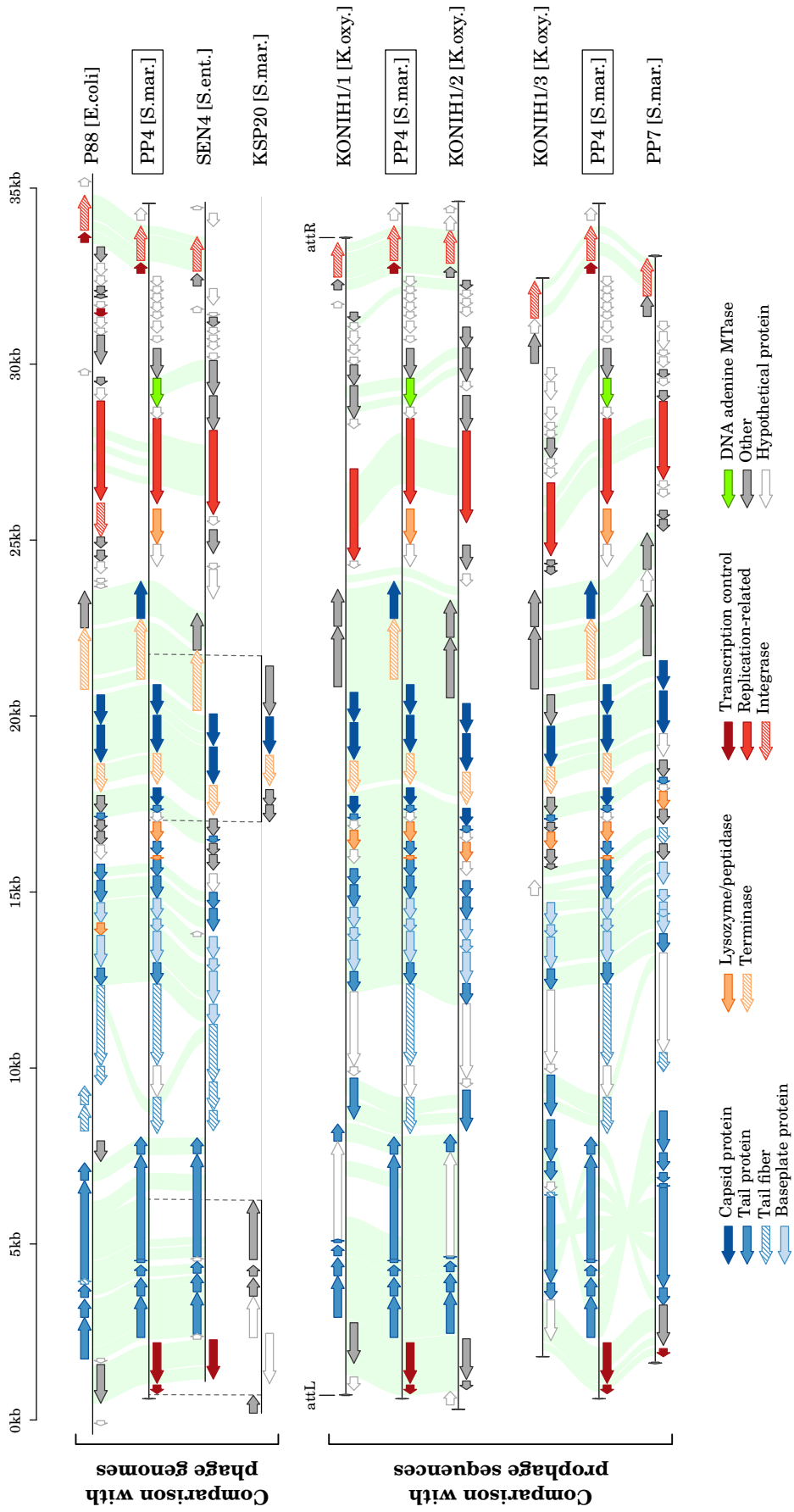

Supplementary Figure S1: Comparison of prophage PP4 with related (pro)phages. P88 and SEN4 infect *Escherichia coli* and *Salmonella enterica*, respectively. KSP20 infects *S. marcescens* (only two sequence fragments available). KONIH1/1-3 are three prophages identified in the genome of a *Klebsiella oxytoca* strain. PP7 is another prophage candidate identified in the genome of the *S. marcescens* strain used in our study but for which no induction was detected. Matches found with `tblastx` are highlighted in green. See details about the search for sequences related to PP4 in Methods.

820

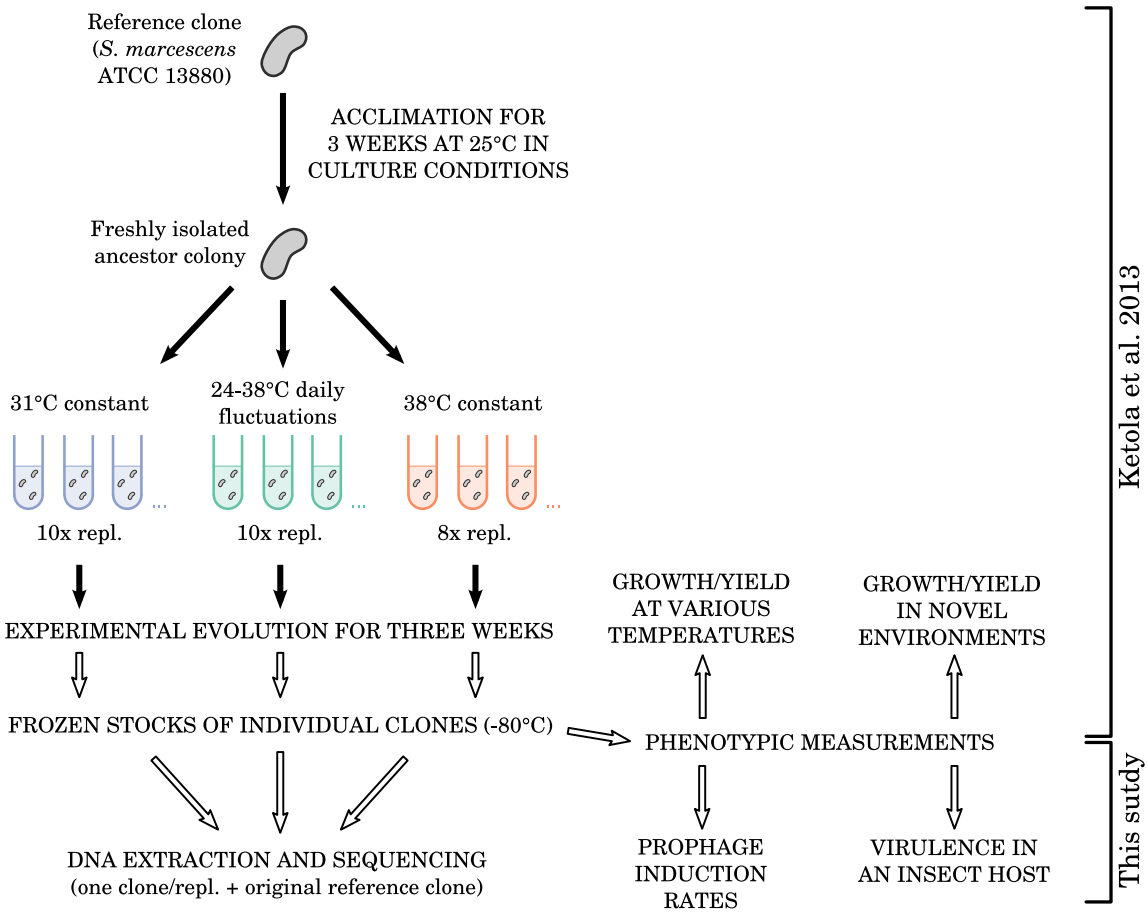

Supplementary Figure S2: Setup of the evolution experiment from which clones were isolated. One randomly selected clone per evolved population was used for sequencing. Open arrows after experimental evolution indicates steps where evolved clones were grown under common garden conditions. Details of the evolution experiment are available in Ketola et al. 2013 (Ketola et al., 2013).

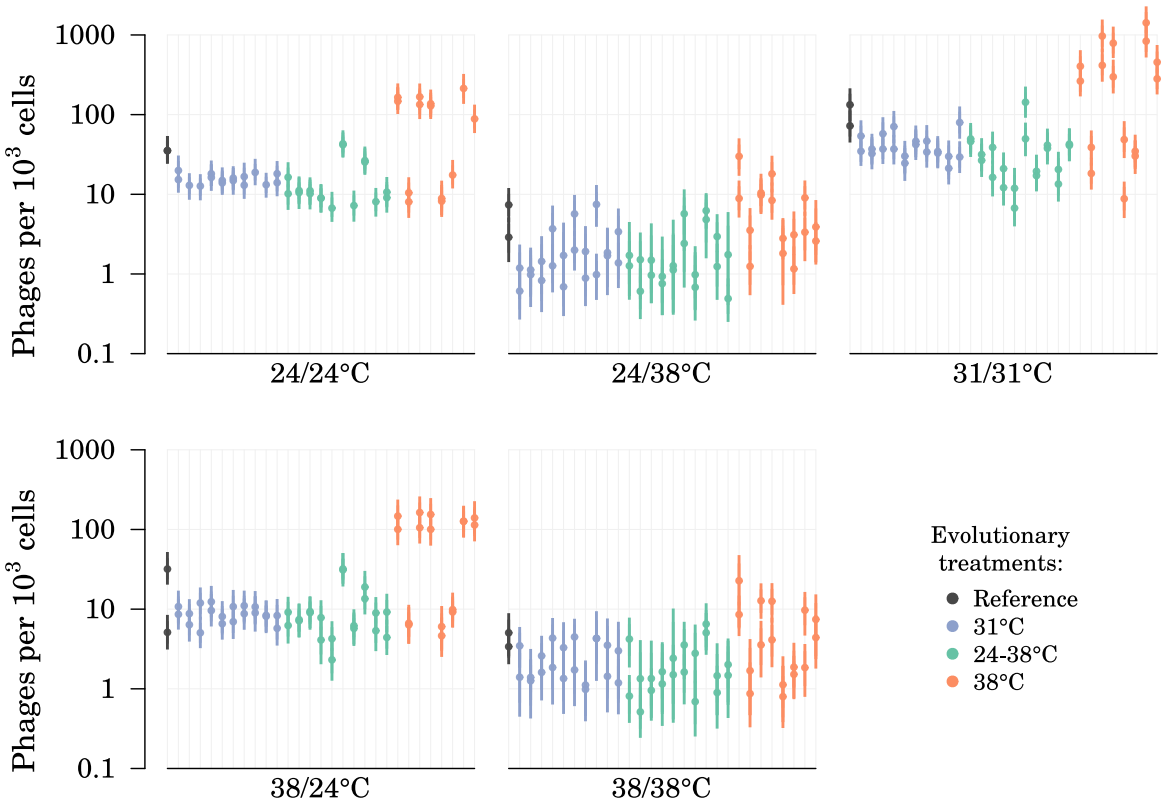

Supplementary Figure S3: Estimated induction rates of prophage PP4 per evolved strain per assay. For each strain in each assay, two replicate measurements are available in most cases. Estimated prophage induction rates are shown as posterior mean and 95% credible interval for each measurement.

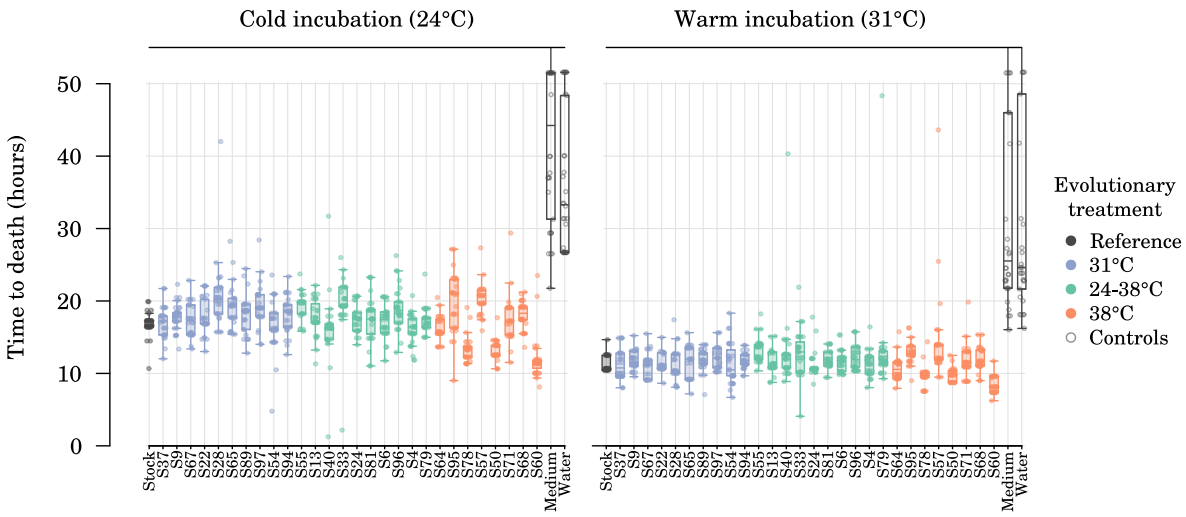

Supplementary Figure S4: Longevity of waxmoth larvae at two incubation temperatures after injection with experimental *Serratia marcescens* strains. Each vertical lane shows larvae injected with a given strain. The Medium and Water lanes show control larvae injected with sterile medium and sterile water, respectively. Longevity is corrected for the effect of replication blocks, culture optical density and larva body mass. Dots are individual larvae. Boxplots center line, median; box limits, upper and lower quartiles; whiskers extend to the most extreme data points which are no more than 1.5 times the interquartile range away from the box.

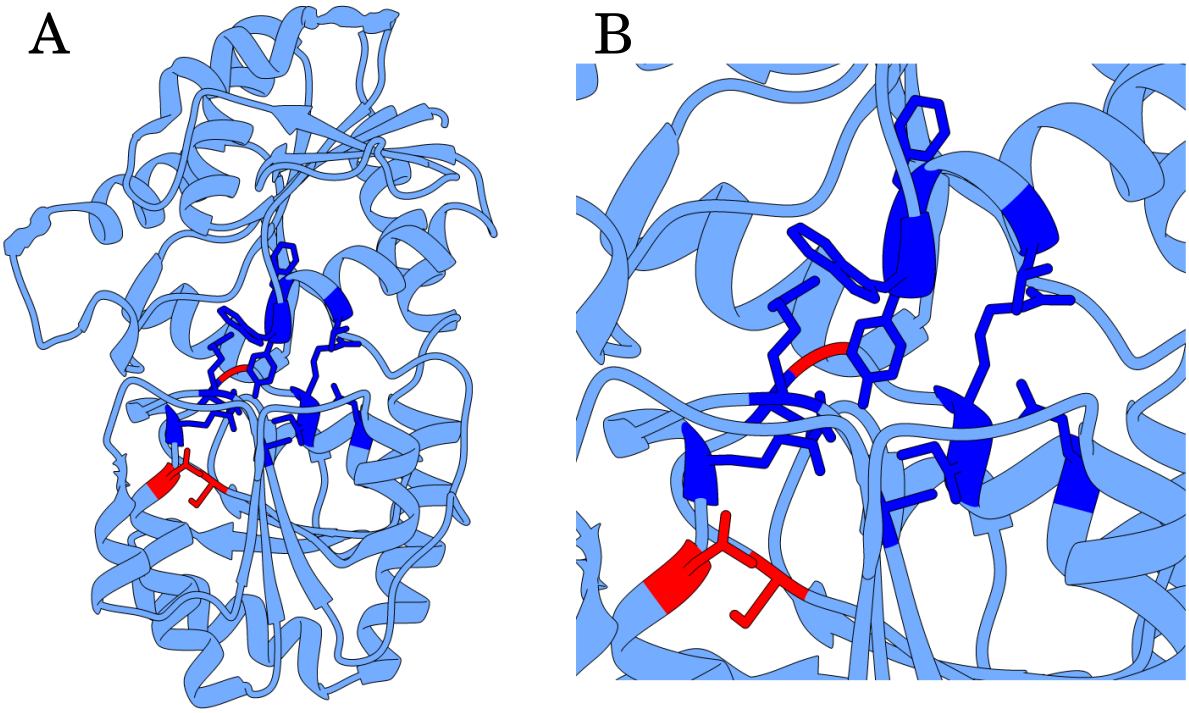

Supplementary Figure S5: Location of observed amino acid substitutions in the predicted structure of a glycosyltransferase of *Serratia marcescens* (GenBank record QSP20947.1). The predicted protein is 380 amino-acid long and its structure was modelled using the Phyre2 online server (Kelley et al. (2015); "intense mode" run submitted on 2015-10-26). A) Overview of the tertiary structure of the complete monomer; B) close-up of the putative active site. Blue, amino-acids which have a side chain close to the ligand site, based on a protein of related structure (PDB 3mbo, Parsonage et al. (2010)); red, amino-acids which exhibited three independent mutations in the evolved strains in our experiment (mutations *28*, *29* and *30* in Supplementary Table S2).

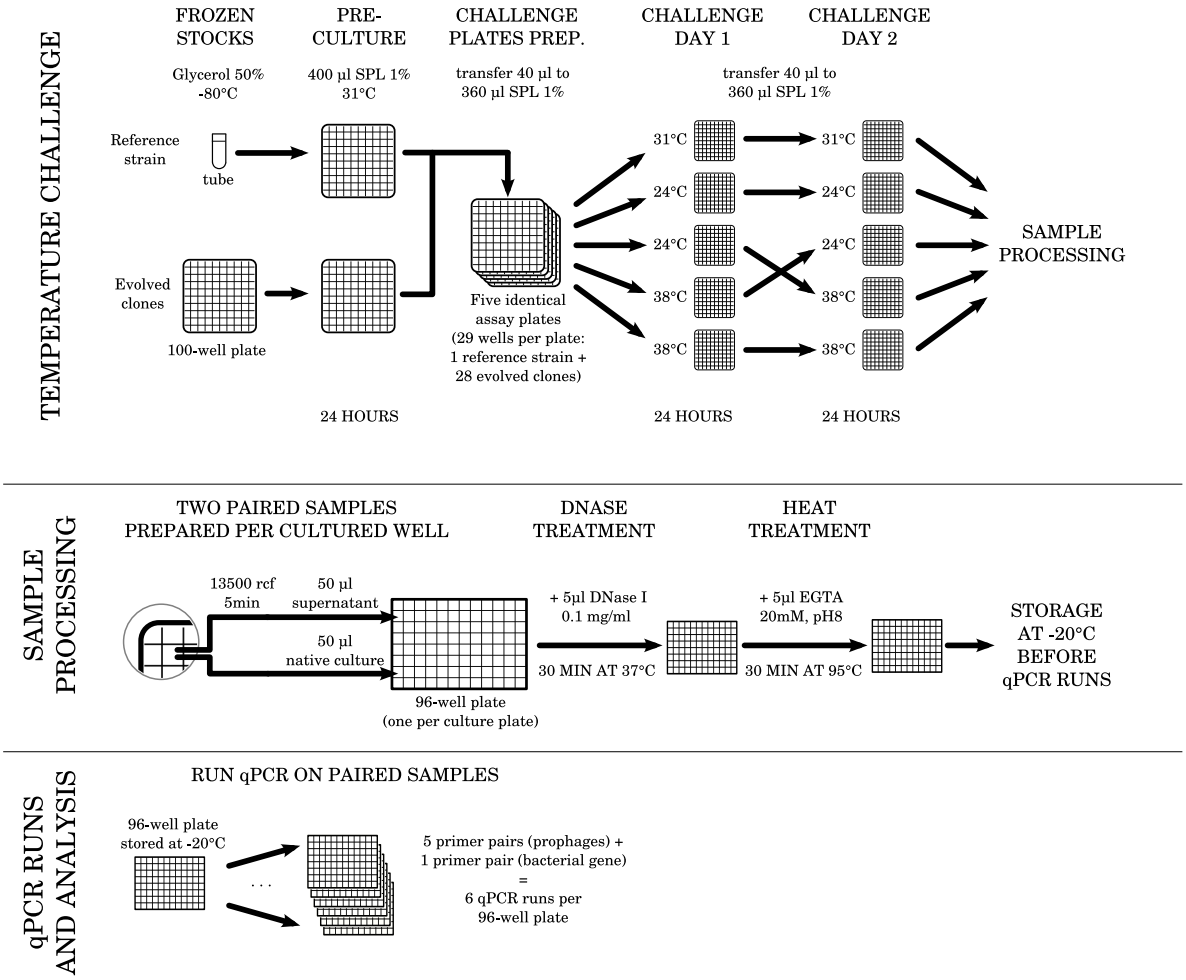

Supplementary Figure S6: Overview of the experimental protocol used for the prophage induction assays. The prophage primers used in the qPCR runs were for prophages 1, 3, 4, 6 and 7, after preliminary experiments with the reference strain showed no detectable amount of extra-cellular DNA for prophages 2 and 5.

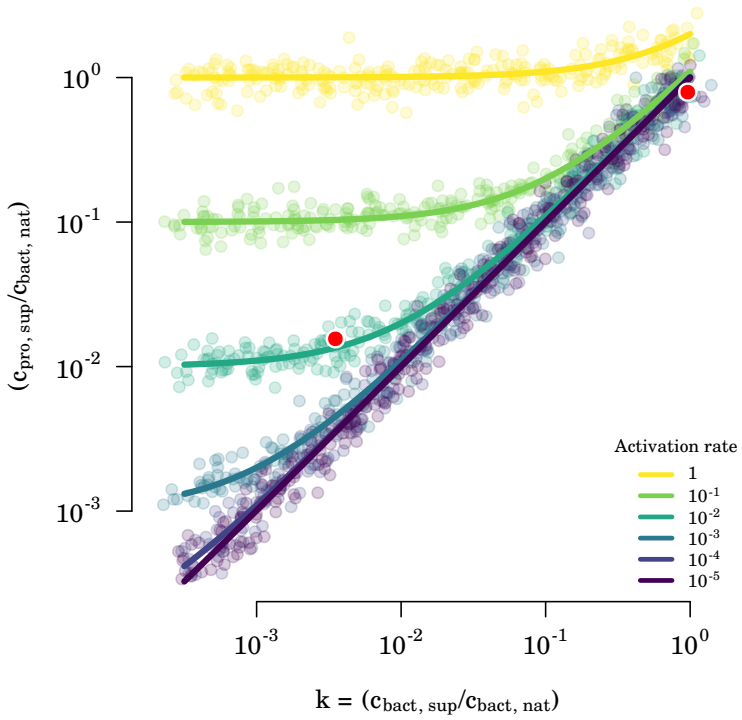

Supplementary Figure S7: Simulation of qPCR results for different prophage activation rates a and different centrifugation concentration factors k. $c_{bact,nat}$, $c_{bact,sup}$ and $c_{pro,sup}$ are the qPCR quantifications of DNA copie numbers for bacterial gene in native and supernatant samples and for prophage gene in supernatant samples, respectively. The colored lines show the predicted trajectories of $c_{pro,sup}/c_{bact,nat}$ versus $c_{bact,sup}/c_{bact,nat}$ from native samples (top-right corner) towards supernatant samples (to the left) as the centrifugation concentration factor k decreases (i.e. as supernatant samples are more and more impoverished in bacteria cells). The shape of the trajectories depends on the activation rate of the prophage, i.e. on how many phage particles are present per bacteria cells in the native sample. The colored dots matching the colored predicted trajectories represent simulations of qPCR estimations which would be obtained as the centrifugation removes more and more bacteria cells from the supernatant, assuming a precision of the Cq values $\sigma_{cq} = 0.48$ and triplicates qPCR measurements for each culture well, as was done in our experiment. As can be seen on the figure, the sensitivity threshold to detect phage particles decreases as the depletion of bacteria cells becomes more complete. However, even at k values of 10^{-3}, activation rates of 10^{-4} and lower are not distinguishable from the absence of induction. The red dots represent the results for a hypothetical culture, with the top-right dot representing the native sample and the bottom left dot representing the supernatant sample.